409115

40 P

Vertical Photon Transport in Cloud Remote Sensing Problems

S. Platnick

Joint Center for Earth Systems Technology,
University of Maryland Baltimore County, Baltimore, Maryland
and
NASA/Goddard Space Flight Center, Greenbelt, Maryland

For submission to: *Journal of Geophysical Research–Atmospheres*
27 August 1999

Corresponding author address:

S. Platnick
Code 913
NASA GSFC
Greenbelt, MD 20771
platnick@climate.gsfc.nasa.gov

Abstract

Photon transport in plane-parallel, vertically inhomogeneous clouds is investigated and applied to cloud remote sensing techniques that use solar reflectance or transmittance measurements for retrieving droplet effective radius. Transport is couched in terms of weighting functions which approximate the relative contribution of individual layers to the overall retrieval. Two vertical weightings are investigated, including one based on the average number of scatterings encountered by reflected and transmitted photons in any given layer. A simpler vertical weighting based on the maximum penetration of reflected photons proves useful for solar reflectance measurements. These weighting functions are highly dependent on droplet absorption and solar/viewing geometry.

A superposition technique, using adding/doubling radiative transfer procedures, is derived to accurately determine both weightings, avoiding time consuming Monte Carlo methods. Superposition calculations are made for a variety of geometries and cloud models, and selected results are compared with Monte Carlo calculations. Effective radius retrievals from modeled vertically inhomogeneous liquid water clouds are then made using the standard near-infrared bands, and compared with size estimates based on the proposed weighting functions. Agreement between the two methods is generally within several tenths of a micrometer, much better than expected retrieval accuracy. Though the emphasis is on photon transport in clouds, the derived weightings can be applied to any multiple scattering plane-parallel radiative transfer problem, including arbitrary combinations of cloud, aerosol, and gas layers.

1. Introduction

Knowledge of cloud droplet sizes is important in physical and radiative cloud process studies, climate modeling, and investigations of potential cloud-climate feedbacks [c.f. *Wielicki et al.*, 1995 for review]. For example, droplet size is influenced by both droplet concentration and water content. Droplet concentration is in turn affected by cloud condensation nuclei concentrations present during nucleation, providing a link between droplet sizes and cloud albedo via the so-called indirect effect of aerosols on climate mechanism and cloud susceptibility [*Charlson et al.*, 1987; *Twomey*, 1974; *Twomey*, 1991]. The influence of droplet concentration on precipitation processes, and subsequent consequences to cloud fraction and lifetime is also of interest [*Albrecht*, 1989; *Austin et al.*, 1995; *Pincus and Baker*, 1994]. In general circulation models (GCMs), droplet size is used for the parameterization of cloud optical thickness from liquid water path. Several studies have shown GCM radiation budgets to be sensitive to droplet size due to this parameterization [*Kiehl*, 1994; *Slingo*, 1990]. All of these issues have helped spur interest in the remote sensing of cloud droplet size.

In radiative studies, it is the effective radius ($r_e = \overline{r^3} / \overline{r^2}$) that is the important measure of the droplet size distribution. Solar reflectance measurements in visible and near-infrared atmospheric window bands can be used to infer cloud optical thickness and effective radius. The droplet size information is obtained with one of the water-absorbing near-infrared bands, usually located in the 1.6, 2.2, or 3.7 μm spectral region. These retrievals presume the existence of vertically homogeneous, plane-parallel clouds, in which case retrievals made with each near-infrared band should report the same droplet effective radii. However, both theory and in situ measurements show clouds to exhibit a measurable droplet size vertical structure; measurements and satellite imagery also indicate horizontal inhomogeneities over many scales [e.g., *Cahalan and Snider*, 1989; *Gerber et al.*, 1994]. Since transport will be shown to be highly dependent on the amount of liquid water absorption in the band, inhomogeneous clouds may lead to differences among the individual near-infrared retrievals. Retrievals using an airborne imaging radiometer flown over marine stratocumulus clouds have shown that significant differences can occur among the three near-infrared bands [*Platnick et al.*, 1999]. Though fundamental sources of retrieval error may have been responsible (e.g., instrument calibration), it is possible that cloud inhomogeneities were a contributing factor.

In investigating the sensitivity of cloud retrievals to cloud inhomogeneities, it is convenient to consider the vertical and horizontal scales separately. The current work focuses on vertical photon transport; approximations for horizontal transport were previously discussed [*Platnick*, 1996; *Platnick*, 1999a]. It is useful in remote sensing problems to couch vertical transport through plane-parallel layers in terms of a weighting function which approximates the relative information content of each layer to the overall reflected or transmitted signal. For cloud remote sensing, this primarily means information regarding layer droplet size (related to droplet absorption). Though weighting functions in single scattering problems are exact, any weighting for a multiple scattering problem can only be approximate. Several weightings are investigated in this paper, including one based on the average number of scatterings encountered by reflected and transmitted photons in any given layer. A superposition technique, using basic adding/doubling radiative transfer procedures, is derived to accurately and quickly determine the number of layer scatterings, avoiding time consuming Monte Carlo calculations. A simpler vertical weighting based on the maximum depth achieved by reflected photons proves useful for solar reflectance measurements.

In summary, we will investigate vertical photon transport in plane-parallel, vertically inhomogeneous clouds with direct application to cloud remote sensing problems that use solar reflectance or transmittance measurements to infer cloud droplet size. This is an extension to an earlier preliminary work [*Platnick*, 1996]. We begin in section 2 with a discussion of the physics behind cloud droplet size retrievals, the use of 1.6, 2.2, and 3.7 μm near-infrared spectral bands, and the basic implementation of the algorithm which presupposes homogeneous clouds. Analytic models are then developed for prescribing cloud droplet size as a function of cloud height or optical depth in section 3. These cloud models are used in later sections for assessing the effect of various droplet size profiles on retrievals and weighting functions. Candidate vertical weighting functions are proposed and discussed in section 4. Calculations of the vertical weighting functions using derived superposition formulae are made for bidirectional reflectance and transmittance remote sensing problems at various combinations of solar and viewing angles, as well as for flux measurements. Selected results are compared with Monte Carlo calculations. In section 5, retrievals made with the three near-infrared bands are presented for several cloud models and compared with size estimates based on the weighting functions. Conclusions regarding the impact of vertical structure on retrievals can then be made. The possibility of inferring the droplet size profile from the three retrievals via an inversion technique is discussed in section 6. Since the discussion is limited to transport through plane-parallel cloud layers, we will often drop the geometric qualifier to keep the language more concise. Unless otherwise mentioned, an *inhomogeneous* cloud will refer to a cloud consisting of various plane-parallel layers, each having different radiative properties.

2. Cloud Microphysical Retrievals

Simultaneous cloud microphysical and optical thickness retrievals using solar reflectance measurements, along with in situ validations, began with *Twomey and Cocks* [1982; 1989], *Foot* [1988], *Nakajima and King* [1990], and *Nakajima et al.* [1991]. Though the physical basis for these retrievals is important in understanding the effects of photon transport, only a summary will be attempted here.

Retrieval algorithms make use of multispectral information contained in bands that are absorbing and non-absorbing for cloud particles. Since useful bands are located in atmospheric windows to minimize the effect of molecular absorption, further mention of absorption will be understood to refer to water particles and not water vapor or other gases. Though we limit our discussion to clouds with liquid water droplets, the algorithms can, at least in principle, also be applied to ice clouds [e.g., *Ou et al.*, 1995; *Young et al.*, 1998]. Non-absorbing bands include atmospheric windows from the visible up to 1.2 μm, each with particular advantages depending on underlying surface type or amount of Rayleigh scattering. Reflectance in these bands depends primarily on cloud optical thickness with only a small dependence on droplet size, mainly through the droplet scattering asymmetry parameter. That is, a family of effective radius curves on a reflectance versus optical thickness plot would very nearly overlap each other. Reflectance measurements in these bands can therefore be used to help infer optical thickness. Unless otherwise stated, reflectance will refer to the bidirectional quantity (i.e., a function of both solar and viewing directions) and not albedo, or hemispheric flux reflectance (a function of solar direction only). For conservative scattering, cloud reflectance increases monotonically with optical thickness towards a limiting value near unity, though not necessarily exact unity for bidirectional reflectance.

The useful absorbing bands are centered around 1.6, 2.2, and 3.7 μm, with the longer wavelength bands having the greater absorption. These will be referred to collectively as near-infrared bands (also referred to as shortwave and midwave infrared

bands). In each near-infrared band, droplet absorption increases with cloud droplet size over the expected size range. The greater the droplet absorption the less the cloud reflectance, all else being equal, and so near-infrared reflectance measurements contain information about droplet effective radius. However, the near-infrared reflectance may also have significant dependence on optical thickness. Thin clouds provide little cumulative absorption to reflected photons because of the relatively small number of scatterings which can occur, and so reflectance is highly dependent on optical thickness. As a cloud becomes thicker, the near-infrared reflectance eventually reaches an asymptotic limit, potentially much less than unity, as absorption eliminates the possibility that deeply penetrating photons can survive the increasing number scattering events required to return to cloud-top. Beyond this limit, reflectance is constant with optical thickness, leaving only a droplet size dependence. The value of the reflectance limit decreases with increasing absorption (or with droplet size for a given band). The optical thickness corresponding to this reflectance limit also decreases with increasing absorption, ranging from about 5 to 30 for the 3.7 and 1.6 μm bands, respectively. So the 3.7 μm band is the most independent of optical thickness and the 1.6 μm most dependent. In summary, a family of effective radius curves on a near-infrared reflectance vs. optical thickness plot would very nearly overlap for thin clouds and diverge toward different asymptotic reflectances at large thicknesses, the difference being related to effective radius. Simultaneous reflectance measurements in non-absorbing and absorbing bands therefore contain the essential information required to infer both optical thickness and effective radius. A graphical summary of these concepts can be found in the plots of *Nakajima and King* [1990] and *Platnick et al.* [1999].

Solar retrieval algorithms compare measured reflectances in absorbing and non-absorbing bands with calculated reflectances derived from homogeneous, plane-parallel cloud models. These modeled reflectances are usually in the form of libraries which span the expected range of cloud optical thickness, droplet effective radius, and solar and viewing geometry. The retrieved optical thickness and effective radius corresponds to the library reflectances (from at least one absorbing and non-absorbing band) which are collectively closest, in some sense, to the measured reflectances. Since the libraries are modeled after clouds which are uniform in both the vertical and horizontal, retrievals of real-world clouds can be considered the plane-parallel, homogeneous equivalent quantities. That is, the retrievals give the parameters of a homogeneous cloud having nearly the same reflectances as the measured cloud for the particular geometry. Various implementations of this basic approach with the 1.6 and 2.2 μm bands are described in the literature [*Nakajima and King*, 1990; *Rawlins and Foot*, 1990; *Twomey and Cocks*, 1989]. The 3.7 μm band retrievals are complicated by cloud thermal emission which can be a potentially significant part of the measured radiation. Since cloud emissivity will vary with droplet absorption, thermal emission is a function of droplet size in addition to temperature. An algorithm must therefore search for the effective radius that gives a total above-cloud intensity consistent with both solar reflectance and cloud emission. Satellite retrievals with this band include *Arking and Childs* [1985], *Platnick and Twomey* [1994], *Han et al.* [1994], *Platnick and Valero* [1995]. It has also been demonstrated that there is size information in cloud emissivity at longer wavelengths [*Ackerman et al.*, 1995; *Parol et al.*, 1991].

A similar approach can be attempted with transmittance [*Rawlins and Foot*, 1990] though these measurements (either bidirectional or flux) have much less dependence on effective radius for both absorbing and non-absorbing bands. There are several reasons for this. First, all transmittance curves must start and end at the same value regardless of wavelength or cloud microphysics (e.g., flux transmittance goes from unity in the absence of a cloud to zero for infinitely thick clouds). This is in contrast to near-infrared reflectance curves which, as the cloud becomes optically thicker, monotonically approach different limiting reflectance values depending on wavelength and effective radius. So in the two extreme optical thickness limits, there is no possible cloud information in a transmittance measurement. Secondly, at intermediate thicknesses, the increase in forward scattering with droplet size tends to cancel the accompanying increase in droplet absorption and, once again, little microphysical information is available compared to reflectance measurements. However, for the same reasons, transmittance in any one of the remote sensing bands is capable of reasonably good optical thickness retrievals.

In the remaining sections, we will discuss photon transport in reflectance, transmittance, and emittance problems. However, the emphasis will be on reflectance-based effective radius retrievals of stratus clouds. These plane-parallel-like clouds are most likely to be compatible with retrieval cloud models, but may still have significant vertical inhomogeneities across the scales of photon transport. These inhomogeneities may lead to errors or biases in the retrieved cloud effective radius. Clearly, there are other potentially significant and more fundamental sources of retrieval error, such as uncertainties in the calculation of homogeneous cloud reflectances, instrument error, and atmospheric conditions, to name a few [e.g., *Han et al.*, 1995; *Han et al.*, 1994; *Platnick and Valero*, 1995]. There is also an unexplained tendency for size retrievals to be

significantly larger than in situ measurements, i.e., anomalous absorption [*Nakajima et al.*, 1991; *Twomey and Cocks*, 1989]. It is within this overall context that effects of cloud inhomogeneities should also be examined. A better understanding of retrieval uncertainty is especially important given the interest in global droplet size climatologies [*Han et al.*, 1994; *King et al.*, 1992].

3. Vertical Cloud Structure

Cloud retrievals are based on vertically homogeneous cloud models. However, it is known from both simple theoretical models and empirical data that cloud droplet sizes are likely to increase significantly with height in a non-precipitating cloud. From theoretical considerations, an adiabatic cloud profile has liquid water content increasing linearly with height over large thicknesses. To the extent that droplet numbers have been found to be relatively constant with height , droplet sizes would also increase with height. A number of in situ measurements of cloud droplet size and/or liquid water content vertical profiles have been reported [*Austin et al.*, 1995 for midlatitude stratocumulus; *Curry*, 1986 for arctic stratus; *Garrett and Hobbs*, 1995; *Gerber et al.*, 1994; *Nicholls and Leighton*, 1986; *Noonkester*, 1984; *Slingo et al.*, 1982; *Stephens and Platt*, 1987]. As an example, *Garrett and Hobbs* [1995] measured effective radius increases at cloud top relative to cloud base of about 50% and 100% in two stratocumulus case studies near the Azores. However, it is difficult to obtain statistically meaningful profiles which would require sufficient sampling at all levels in the same cloud region, and so profile measurements often appear quite noisy. Nevertheless, most clouds appear to have liquid water content profiles that are sub-adiabatic to some extent, especially near cloud top [e.g., *Nicholls and Leighton*, 1986], therefore having less drastic size increases with height compared to an adiabatic cloud, though still potentially significant. Droplet size profiles sometimes have a non-linearity suggestive of adiabatic, or near-adiabatic, liquid water content profile . In other cases, droplet sizes seem to increase linearly with height. Several analytical models for droplet size profiles are derived momentarily.

Due to varying absorption, microphysical retrievals made with different near-infrared bands will sample different vertical portions of the cloud and infer different effective radii. A retrieval in any given band represents the average radiative effect of the droplet size profile for that band. A reflectance measurement in the 1.6 μm band is least affected by absorption and can contain information regarding droplet sizes in relatively deep layers of the cloud. The 2.2 and 3.7 μm bands have progressively more absorption and the vertical sampling is more shallow. Clearly, assigning a single effective radius to an entire cloud may be rather ambiguous from the remote sensing standpoint, especially when using multiple near-infrared bands. Of course, the concept of a "correct" size retrieval is only meaningful in terms of the intended application (e.g., determination of liquid water path, broadband fluxes, influence of CCN, etc.).

3.1. Analytic Droplet Size Profiles

We wish to derive models for cloud droplet size profiles for use in assessing the impact of vertical structure on effective radius retrievals and the utility of vertical weighting functions discussed in the next section. The vertical structure will be given by simple analytic profiles derived from various prescribed physical constraints, and not from cloud dynamic and microphysical models.

The following nomenclature is used: the vertical variable for the radiation problem is *optical depth*, τ, measured from cloud top downward, while the term cloud *optical thickness*, τ_c, is used to indicate the overall optical depth down to cloud base. For instance, we may refer to a level at an optical depth of 5, in a cloud with an optical thicknesses of 10. We therefore require a specification of effective radius as a function of optical depth for a given optical thickness, i.e., $r_e(\tau,\tau_c)$. In terms of geometrical height, z, which will be defined to increase from zero at cloud base to h at cloud top, optical depth at a wavelength λ, is given by

$$\tau_\lambda(z) = \int_z^h dz' \int_0^\infty Q_{e_\lambda}(r)\pi r^2 n(r,z')dr \approx \int_z^h 2\pi \overline{r^2}\, N(z')dz', \qquad (1)$$

where the extinction efficiency, $Q_{e\lambda}(r)$, is approximately 2 for cloud droplet size particles at the wavelengths of interest, and $N(z)dz$ is the total droplet concentration in the differential layer between z and $z+dz$.

First, consider an adiabatic cloud. Liquid water content, *LWC*, in a saturated adiabatic process increases linearly with geometric height for lower clouds and over extended thicknesses. Therefore, adiabatic cloud liquid water at the height z is given as

$$LWC = C\int_0^\infty r^3(z)n(r,z)dz = C\overline{r^3(z)}N(z) \sim z, \qquad (2)$$

where $C=4\pi\rho_l/3$ and ρ_l is the density of liquid water. Ignoring the differences between the area-weighted radius, volume-weighted radius, and effective radius [*Martin et al.*, 1994], we can rewrite Eq. 2 as $r_e^3(z)N(z) = c_0 + c_1 z/h$, where c_0 and c_1 are constants. Assuming N is constant with height, $r_e(z) \propto (c_0 + c_1 z/h)^{1/3}$. A curvature of this type (second derivative less than zero) is often seen in measured profiles [e.g., *Stephens and Platt*, 1987]. Differentiation yields $dz \propto N r_e^2(z)dr_e$. Substituting this expression for dz into the second form of Eq. 1, and integrating over r_e from $r_e(z)$ to the cloud-top droplet effective radius, r_{top}, gives $\tau \propto (r^5_{top}-r_e^5(z))$. The size profile can now be expressed in terms of optical depth instead of geometric height. Rearranging gives $r_e(\tau,\tau_c) = (a_0 - a_1\tau/\tau_c)^{1/5}$ where the constants $a_0=r^5_{top}$ and $a_1= r^5_{top}-r^5_{base}$ are determined from prescribed boundary conditions on droplet size, with r_{base} as the cloud base effective radius. Though cloud base should be strictly defined as the level where liquid water content and droplet size become zero, the location of cloud base from in situ measurements is ambiguous due to sampling difficulties, uncertainty associated with the measurement of small liquid water content and droplet sizes, and the rapid increase in droplet size over relatively small vertical scales. In addition, these thin bottom layers with small droplet sizes make the least contribution to cloud optical thickness. For these reasons, a well-defined cloud base with a non-zero boundary condition is used. An example of an adiabatic droplet size profile as a function of both optical depth and height is shown in Fig. 1 for $\tau_c=8$, $r_{base}=5$ μm, and $r_{top}=12$ μm. Droplet sizes are seen to quickly increase with height from cloud base. The linear liquid water content profile is also shown. Boundary conditions are consistent with a droplet concentration of about 60 cm^{-3}. Analytic formulae for the adiabatic cloud model are summarized in Table 1 (profile *B*).

A sub-adiabatic liquid water content profile, having adiabatic liquid water near cloud base but with increasing entrainment, or drying, towards cloud top can also be described. In this case, liquid water can be specified with the power law $(c_0 + c_1 z/h)^x$, where $0<x<1$ and c_0, c_1 are again constants determined from prescribed boundary conditions. Equations for the droplet size profiles are given in Table 1 (profile *A*). An example with $x=0.75$ is shown in Fig. 1 as the *sub-adiabatic aloft* profile. The reduction in cloud top liquid water results in relatively less change in droplet size in the upper portions of the cloud. Note that curves in Fig. 1 have identically prescribed boundary conditions. For clouds forming in otherwise identical conditions, the sub-adiabatic cloud would of course have a smaller cloud-top liquid water content boundary condition than the adiabatic cloud and therefore less water and smaller droplet sizes at all levels. Prescribing equivalent liquid water content in the lower parts of the cloud, the sub-adiabatic model with x=0.75 gives a cloud top liquid water content about 60 % less than the comparable adiabatic cloud.

Measured droplet size profiles are usually quite noisy and often appear to be linear with height [e.g., *Stephens and Platt*, 1987]. Following the same procedure as for the adiabatic cloud, it can be shown that $r_e(z)\sim z$ implies $LWC\sim z^3$ and $r_e(\tau,\tau_c) = (a_0 - a_1\tau/\tau_c)^{1/3}$. The result is an analytic form similar to the adiabatic and sub-adiabatic profiles as shown in Table 1 (profile C). For the same prescribed boundary conditions, this profile represents a cloud with sub-adiabatic liquid water content at midlevels (i.e., the occurrence of a drying process in middle layers) and droplet sizes decreasing more rapidly with cloud depth in the upper part of the cloud than for the adiabatic profile, i.e., larger dr_e/dz or $dr_e/d\tau$ at upper levels (see Fig. 1). Though the size profile is recognizable in measurements, the accompanying liquid water profile is not obvious in the in situ profiles previously cited and may not be realistic except for perhaps multilayer or decoupled cloud layers. A profile with droplet size decreasing even more rapidly with depth in the upper part of the cloud can be found by simply specifying droplet size to be linear in optical depth, i.e., $r_e(\tau,\tau_c) = a_0 - a_1\tau/\tau_c$, implying $LWC\sim z^5$ and $r_e(z)\sim z^{5/3}$ (profile D in Table 1). This profile gives the largest upper level $dr_e/d\tau$, providing a useful test of the weighting function formulations in the next section.

Table 1 and Fig. 1 summarizes the four analytic profiles discussed. Consider a reflectance-based size retrieval. Regardless of the assumed profile, droplet size retrievals will differ in each of the near-infrared bands due to differences in droplet absorption which increases with band wavelength. A reflection measurement at 1.6 µm, perceiving the least absorption, contains information from deeper cloud layers than 2.2 and 3.7 µm measurements and so infers a smaller effective radius. Likewise, the 2.2 µm size retrieval will be smaller than the 3.7 µm retrieval. For reflectance, all bands sample the upper portions of the cloud more readily than lower parts, even for a band with no absorption (e.g., in the visible). It is the profile of droplet size with respect to optical depth in the upper parts of the cloud that has the most influence on retrieval size and band differences. For the same prescribed boundary conditions, a profile having small values for the derivative $dr_e/d\tau$ in upper portions of the cloud will have sizes more nearly constant with

optical depth implying larger retrievals and smaller retrieval differences among the near-infrared bands. Therefore, all near-infrared bands will infer the largest droplet size for the *sub-adiabatic aloft* profile, where $dr_e/d\tau$ is smallest in upper portions of the cloud (see upper plot of Fig. 1); retrievals for the adiabatic profile would not be much less. Size retrievals would be smallest for the $r_e(\tau,\tau_c) \propto \tau$ profile which has the largest values of $dr_e/d\tau$ in upper portions of the cloud. Near-infrared retrieval differences would also be greatest for this profile making it helpful for assessing the robustness of weighting functions.

Four example test clouds, based on the adiabatic and $r_e(\tau,\tau_c) \propto \tau$ profiles (B and D in Table 1), are used in much of the subsequent analyses. These two profiles provide a useful range in the size profile, specifically $dr_e/d\tau$ at upper levels. Table 2 summarizes the four test clouds for both profiles. The test cloud optical thicknesses range from a relatively small τ_c=5 to a moderately thick τ_c=15. Clouds with thicknesses less than τ_c=5 will not have a significant vertical signature. Clouds up to τ_c=15 span the optically thick limit for 2.2 and 3.7 µm band reflectances (see section 2); lower layers will be inconsequential in these bands for thicker clouds. The thickest cloud is assigned the smaller droplet sizes (less droplet absorption) to allow lower layers some influence on reflectance. The range of radii from cloud top to base is somewhat larger than typical in situ measurements, but still realistic. For numerical purposes, the test clouds are built up from individual homogeneous layers with optical thicknesses of 0.25 and integer values of effective radii. Liquid water path is determined from the summation of the product of layer optical thickness and effective radius (Eqs. 1 and 2 give the water path in layer i as $2r_{e,i}\Delta\tau_i/3$, in units of g m^{-2} for r_e in micrometers). Other microphysical quantities such as liquid water content, LWC, and droplet concentration, N, cannot be uniquely determined from specification of optical thickness and droplet sizes alone. Liquid water content requires knowledge of N, and only the product Nh is specified (Eq. 1). Recall that N is assumed constant with height in all analytic models. Table 2 gives values of N and LWC if all clouds have a geometric thickness of 0.3 km. The small values of N, representative of pristine air conditions, are a consequence of the relatively large prescribed cloud top effective radii. The adiabatic profile has the more reasonable liquid water content at the cloud boundaries, whereas the other profile is much wetter due to larger droplet concentrations. Model results and conclusions are discussed at the end of the next section. Results from the other two analytic profiles were also examined. The $r_e\sim z$ profile (C) is used in many of the weighting function plots.

4. Multiple scattering weighting functions

Two immediate questions come to mind. First, to what extent do the three near-infrared bands infer different effective radii for realistic size profiles? Secondly, do measurements in the near-infrared bands contain information sufficient to infer the size profile? That is, can an inversion technique be devised.

One approach to these questions is to make repeated forward calculations of cloud reflectance (or transmittance, emittance) with various vertical profiles and use the results as input to a retrievals code. However, the exercise would provide limited insight since information is unavailable on the contribution of individual layers to the retrieval result. The lack of layer information would also make it difficult to assess the possibility of implementing an inversion for the size profile. A more useful approach is to understand the radiative contribution that various layers impart to the overall size determination. For a single scattering problem, this is achieved by couching the problem in terms of vertical weighting functions describing the intensity at a boundary in terms of the cumulative contribution of individual layers. A common example is an infrared sounding technique, where the weighting function at some wavelength is derived from the net transmittance between an emitting layer and the top or bottom of the atmosphere. In the solar region, backscattered ultraviolet measurements infer stratospheric ozone profiles with weighting functions given by ozone path absorption. The single scattering condition provides a one-to-one correspondence between the emitted or scattered radiation from some level and the measured signal. In the case of the cloud problem, multiple scattering destroys this correspondence as radiation may scatter in many layers. However, this doesn't exclude the possibility of useful, though approximate, vertical weighting functions being developed for multiple scattering problems.

For the retrieval of cloud droplet sizes, we seek a weighting function, w, defined such that the *retrieved effective radius*, r_e^*, derived from near-infrared solar reflection or transmission measurements of a cloud with known optical thickness, τ_c, can be determined from:

$$r_{e_\lambda}^* = \int_0^{\tau_c} r_e(\tau)\, w_\lambda(\tau,\tau_c)\, d\tau \ . \qquad (3)$$

Both r_e^* and w are shown as wavelength or band dependent, giving a set of inversion-like formula for $r_e(\tau)$. The dependence of the weighting function on $r_e(\tau)$ and solar and viewing geometry is not shown explicitly. The full functional dependence should be written as $w_m(\tau, \tau_c, \mu, \mu_0, r_e(\tau))$ where μ_0 and μ are the cosine of the solar and viewing angles, respectively. We will use the more explicit notation only when needed.

Note that the weighting function is normalized in this definition, i.e., Eq. 3 must give $r_e^* = r_e$ for a droplet size profile that is constant with height. The ability to infer $r_e(\tau)$ ultimately depends on the relative orthogonality of w at the various near-infrared bands (1.6, 2.2, and 3.7 µm). The weighting function needs to capture the multiple scattering nature of the problem. Weightings based on single scattering properties, such as layer extinction or single scattering albedo will not, in general, be sufficient [*McFarquhar and Heymsfield*, 1998]. Several possibilities for an appropriate weighting function exist. We begin with a simple weighting for reflected radiation.

4.1 Weighting by Maximum Vertical Photon Penetration

A weighting proportional to the maximum vertical penetration obtained by photons will capture some aspect of the multiple scattering process for reflected radiation. Such a weighting could, of course, be found from a Monte Carlo calculation where the total fraction of reflected photons penetrating to each layer can be determined. However, such a method is computationally intensive. A faster and more efficient mean of calculating this weighting is through superposition principles based on standard adding/doubling radiative transfer techniques.

Consider the bidirectional reflectance $R(\tau_c)$ from a cloud with optical thickness τ_c, where the dependence on droplet size, and solar and viewing angles is understood. Assume the cloud is over a black surface. The addition of a differential layer $d\tau$ to the base of the cloud results in a reflectance increase of $dR = R(\tau_c + d\tau) - R(\tau_c)$. By definition, dR represents the part of the total reflected signal $R(\tau_c + d\tau)$ contributed by photons that penetrate only as deep as the $\tau_c + d\tau$ layer. Photons penetrating deeper would be absorbed by the black surface, while photons which have all scatterings above the τ_c level do not contribute to dR. Therefore, the ratio $dR/R(\tau_c + d\tau)$ must represent the fraction of all reflected photons that penetrate to a maximum depth between τ_c and $\tau_c + d\tau$. This must also hold true for arbitrary layers within a cloud. That is, $(R(\tau + d\tau) - R(\tau))/R(\tau)$ gives the fraction of all reflected photons that penetrate to a maximum depth between τ and $\tau + d\tau$ in a cloud of total thickness τ_c. Note that $R(\tau)$ is the reflectance from the portion of the cloud above the level τ, i.e., calculated with lower layers absent. A normalized weighting compatible with Eq. 3 is therefore

$$w_m(\tau,\tau_c) = \frac{\frac{dR(\tau)}{d\tau}}{R(\tau_c)}, \qquad (4)$$

where the subscript m signifies a *maximum* penetration weighting. As with reflectance, w_m also has a functional dependence on the effective radius profile, and solar and viewing geometry. It should be noted that the derivative is calculated for a $d\tau$ layer added to the base of the cloud, not the top. This is an important distinction when cloud microphysics varies with height.

The interpretation of w_m as a weighting proportional to maximum photon penetration is valid for a black surface. This is still valid in presence of a reflecting surface if it is understood that the weighting represents the maximum penetration of only the subset of reflected photons that do not scatter off the surface. Accounting for surface-reflected photons is at odds with the weighting definition since all such photons will have passed through the deepest possible cloud level, i.e., cloud base, at least once. The extent to which a known surface reflectance will modify the inference of effective radius, r_e^*, for a vertically inhomogeneous cloud will be discussed later. If the difference between the retrieval with and without a typical surface reflectance is negligible, then Eq. 4 is still directly applicable. However, if the surface significantly modifies the retrieved cloud effective radius, r_e^*, then there should also be a noticeable change in the weighting (Eq. 3).

Calculations are made using the adding/doubling or superposition technique of *Twomey et al.* [1966]. Cloud reflectance for all combinations of selected incoming and outgoing angle bins is described by the scattering matrix S. The elements $S_{i,j}$ give the ratio of intensity (radiance) at the top of the cloud scattered into the $\mu_i \pm \Delta\mu/2$ bin direction due to incident intensity from the $\mu_j \pm \Delta\mu/2$ direction (μ representing the cosine of the zenith angle). Typically, 10 μ-bins of width 0.10 are sufficient for capturing the angular distribution of intensity in the multiple scattering problems of interest. Bidirectional reflectance is proportional to $S_{i,j}/\mu_j$. Note that μ_j is equated with the cosine of the solar

zenith angle (usually represented by μ_0 in continuous angle notation) and μ_i with the viewing angle (usually μ). Reflectance in Eq. 4 can therefore be replaced by elements of S corresponding to the appropriate solar and viewing geometry. Writing angular dependencies explicitly, the weighting can be expressed in this notation as $w_m(\tau,\tau_c,\mu_i,\mu_j) = (dS_{i,j}(\tau)/d\tau)/S_{i,j}(\tau_c)$. For use in Eq. 4, a library of S-matrices were calculated for thin homogeneous cloud layers of optical thickness 0.25, across a range of integer effective radii. Libraries of corresponding diffuse transmittance matrices, **T**, were also calculated. Then the matrices S(τ), needed for calculating reflectances and their derivatives, can be determined from standard adding techniques using the individual layer matrices superimposed according to the prescribed effective radius profile. Azimuthal variations can be included through a Fourier expansion of the scattering matrices, giving a set of harmonic matrices. Only the fundamental, or azimuthal-averaged reflectances are presented in this paper, which should be sufficient for the multiple scattering problems being considered. Because of reciprocity in bidirectional reflectance [*Chandrasekhar*, 1960, p. 172], an exchanging of solar and viewing directions does not change the weighting function, i.e., $w_m(\tau,\tau_c,\mu,\mu_0) = w_m(\tau,\tau_c,\mu_0,\mu)$. A maximum penetration weighting for a reflected flux (albedo) measurement can be calculated in a similar manner; bidirectional reflectance in Eq. 4 is simply replaced by the albedo, which can be found from the S matrix [*Platnick*, 1999b].

An example of the weighting function w_m is plotted in Fig. 2 for profile C. Details of the cloud model are given in the figure caption. The shape of the weighting function will be discussed shortly. Excellent agreement with Monte Carlo calculations, also shown on the plot, confirms the interpretation of Eq. 4 and verifies its numerical implementation.

4.2 Weighting by the Average Number of Photon Scatterings

A weighting proportional to the average number of scatterings experienced by photons in individual cloud layers would seem more capable of accounting for the effect of multiple scattering on retrievals from vertically inhomogeneous clouds. Consider a reflectance-based retrieval. In a Monte Carlo calculation, this weighting can be found from the total number of scatterings encountered by reflected photons in each layer. The normalization is then the total number of reflectance scatterings in the cloud. Dividing the number of scatterings in each layer by the total number of reflected photons gives an alternative expression for the weighting. Now the normalization becomes the *average* number of scatterings for all reflected photons and the weighting is proportional to the average number of reflectance scatterings in each layer. For example, a normalization of 10 would mean that each reflected photon had, on average, 10 scatterings in the cloud. Of course some photons will have had more scatterings and some less. Likewise, the normalized layer average can then be equated with the fraction of reflected photons having a scattering in the layer (this is a useful interpretation). For example, a layer average of 0.5 can be interpreted as meaning that on average, half of all reflected photons had a scattering in that layer. This fraction will be much less than one for thin layers and can be greater than one if the layer is thick enough to generate multiple scattering.

Though this weighting is more involved than w_m, where only the deepest scattering layer encountered by a photon was considered, it remains to be seen whether it provides a better weighting in the sense of Eq. 3. However, unlike w_m, a weighting based on layer scattering can be defined for transmittance as well as reflectance. We designate this weighting by w_N^r where the subscript N signifies a *number* of scatterings weighting and the superscript r refers to a reflectance weighting (superscript t will refer to a transmittance weighting). Monte Carlo calculation are computationally intensive and would limit the utility of the weighting. As before, a much more efficient means of calculating this weighting is also available through superposition principles and is described in detail in *Platnick* [1999b]. A short summary follows.

Consider a cloud consisting of two finite cloud layers which are in general different. A reflected (transmitted) photon may make multiple passes between the two layers en route to cloud top (base). An infinitesimal cloud layer is now imbedded between the two finite layers. The layer can be made arbitrarily thin so that only single scattering encounters are important. That is, the probability of a photon having multiple scatterings within the layer during transits between the finite layers is insignificant by comparison. The differential portion of the reflected intensity consisting of photons having a scattering in the infinitesimal layer located at a depth τ in a cloud of total thickness τ_c, $dR(\tau,\tau_c)$, can then be determined. As usual, the dependence on droplet size profile and solar/viewing geometry is understood. If the total cloud bidirectional reflectance $R(\tau_c)$ is proportional to the total number of reflected photons, then $dR(\tau,\tau_c)$ must be proportional to the number of reflected photons having a scattering in the infinitesimal layer. The ratio $dR(\tau,\tau_c)/R(\tau_c)$ therefore gives the fraction of reflected photons having a single scattering in the infinitesimal layer, a number much less than one. As discussed above, this is also equivalent to the average number of scatterings in the layer for all reflected photons. Integrating this ratio from τ to $\tau+\Delta\tau$ then gives the

total fraction of photons having a scattering between the levels τ and $\tau+\Delta\tau$. This fraction can become greater than one when multiple scattering becomes important. Likewise, the integration also gives the average number of scatterings between those levels. Once again, all calculations are made using the adding/doubling matrix formulation of *Twomey* [1966]. As with the maximum penetration weighting, there is also reciprocity upon exchange of solar and viewing directions for the bidirectional form of this weighting, i.e., $w_N(\tau,\tau_c,\mu,\mu_0)=w_N(\tau,\tau_c,\mu_0,\mu)$ [see, *Platnick*, 1999b].

Examples of a reflectance and transmittance weighting, w_N^r and w_N^t, respectively, for a 2.2 μm channel are shown in Fig. 2. Calculations are for τ_c=8 and effective radius profile C (r_e~z) from Table 1 with cloud top and cloud base effective radii of 12 μm and 5 μm, respectively. Other details are given in the caption. Both superposition and Monte Carlo calculations are shown. The agreement is excellent, establishing the use of superposition formulae in calculating these plane-parallel scattering statistics. The figure also shows the maximum penetration weighting for reflectance, w_m. In both cases, the upper part of the cloud is weighted more heavily then lower portions as expected, with w_N^r being the more extreme. The transmittance weighting is relatively symmetric with optical depth, showing a broad maximum throughout the middle layers of the cloud. Figure 3 shows the weighting functions for three different cloud optical thicknesses, with the same microphysics and geometry of Fig. 2. The small decrease in w_m at cloud top is due to an initial increase in the derivative $dR/d\tau$ (Eq. 4) for thin clouds. In this example, $dR/d\tau$ increases as effective radii decrease, regardless of optical thickness (a result of both decreasing asymmetry parameter and droplet absorption at smaller radii). This explains the slight increase in w_m near cloud base for the thinnest cloud example where smaller effective radii in the lowest layer are contributing incrementally more to the overall reflectance than adjacent layers. The average number of scatterings also agree with Monte Carlo calculations for both reflected and transmitted photons at all optical thicknesses of interest [*Platnick*, 1999b].

5. Retrieval Examples for Vertically Inhomogeneous Clouds

The accuracy of the proposed weightings in estimating reflectance-based retrieved effective radii from vertically inhomogeneous clouds, via Eq. 3, was tested on the cloud models described in Table 2 for cloud effective radii *increasing* with height. Two specifications for the vertical size profile, profiles B (adiabatic) and D (r_e~τ) from Table

1, are used. The latter profile may be physically unrealistic for single cloud layers, but provides the most rapid decrease in droplet size with depth in the upper part of the cloud. So reflected photons sample a greater variation in droplet sizes and, due to the smaller droplets, can penetrate to deeper layers. This profile therefore provides a more demanding test of the weightings compared with the adiabatic model where droplet size decreases more slowly. Four clouds, each with different optical thicknesses and effective radius boundary conditions at cloud base and top, are considered for each profile as discussed in section 3.1. Comparisons between weighting-derived size estimates and the retrieval code are made for each of the three near-infrared bands.

As mentioned, the model clouds were built up from thin homogeneous cloud layers of optical thickness 0.25. Each layer was assigned an effective radius equal to the integer value closest to the profile-specified size at the depth corresponding to the layer midpoint. For example, the cloud model with τ_c=5 consisted of 20 individual layers having effective radii of 8, 9, 10, 11, or 12 µm. Reflectances in the various bands were calculated for the model cloud using the superposition/adding techniques already discussed. These reflectances then served as measurement input to a retrieval code which determined effective radius by matching the model cloud reflectance with entries in a homogeneous cloud reflectance library spanning the expected range of retrieved radii and optical thickness (see Section 2 for more detail).

In the usual implementation of a retrieval algorithm, both an absorbing and non-absorbing band are used so that effective radius and optical thickness can be retrieved simultaneously. However, for the vertically inhomogeneous cloud, this can lead to slight differences between the retrieved optical thickness and the actual thickness. This error in optical thickness may then affect size retrievals. This is most pronounced when using the less absorbing near-infrared bands, with relatively large optical thickness at the asymptotic reflectance limit, in conjunction with thin clouds. To the extent that the weighting function estimation of Eq. 3 implicitly assumes that optical thickness is known, we wish to isolate the size retrieval from its optical thickness dependence. So for consistency, retrievals in the following comparisons are made with the optical thickness specified. However, letting the optical thickness be a variable during the retrievals only had minor impact, typically modifying retrieved effective radii by less than 0.2 µm for the 1.6 and 2.2 µm bands; no differences were found in 3.7 µm size retrievals because of the band's greater absorption. The 3.7 µm band results use the reflectance signal only, i.e., cloud emission in the band can be considered to have been removed without error. Further, all retrievals are made in the absence of an atmosphere and with a black surface

in all bands. The comparisons are shown in Table 3a for a bidirectional reflectance measurement with cosines of the solar and viewing zenith angles of 0.65 and 0.85, respectively. The first column under each profile gives the retrieved effective radius using the retrieval code. The second and third columns estimate the retrieval with Eq. 3 using weightings w_m and w_N^r, respectively. Results are shown for each of the three near-infrared bands.

Several observations can be made regarding the retrievals. First, since effective radius was specified to increase with height, retrieved sizes increase with band wavelength (i.e., water absorption). Secondly, differences between 1.6 and 2.2 µm retrievals are always less than between those bands and the 3.7 µm band retrieval. The magnitude of the size difference depends on cloud thickness and droplet size profile. For the adiabatic profile, this difference ranges from 0.8 to 1.5 µm for the 1.6 and 3.7 µm bands. Differences between 1.6 and 2.2 µm band are smaller, ranging from 0.3 to 0.6 µm. Finally, for otherwise identical clouds, retrievals for size profile *D* are always less than for the adiabatic profile as expected and differences between the near-infrared retrievals are larger by more than several micrometers. Conversely, the more realistic sub-adiabatic aloft profile (profile *A* in Table 2) would result in slightly larger retrievals in all bands than the adiabatic profile, and differences between the bands would be somewhat smaller.

Both weightings do a good job in approximating the retrieved radius, and are practically equivalent in the 3.7 µm band. However, the maximum penetration weighting, w_m, gives the best retrieval estimate for all bands and over a wide range of cloud thicknesses and droplet sizes. The average number of scatterings weighting, w_N^r, weighting tends to overestimate the retrieved size more than w_m. This is somewhat surprising given the higher order scattering information contained in the weighting. In an attempt to reduce the size estimate, various modifications to the w_N^r weighting were considered, including one proportional $N_i \varpi_{0i}^{N_i}$, where ϖ_{0i} is the layer single scattering albedo. This modification typically reduced the size estimates by only a tenth of a micrometer, leaving the w_m estimate as the preferred weighting. Fortunately, the w_m weighting also has the advantage of being the simplest to calculate. For all cloud models in Table 3a, differences between w_m size estimates and retrievals for the adiabatic profile are within 0.3 µm for the 1.6 µm band, and within 0.1 µm for the 2.2 and 3.7 µm bands. These differences are small compared with estimates of size uncertainty based on homogeneous cloud retrievals [*Platnick and Valero*, 1995]. The sub-adiabatic aloft profile results in slightly smaller differences (not shown). Profile *D* provides the most demanding test of the weighting function. Now, size differences are within 0.9, 0.2, and

$0.2\,\mu m$ for the 1.6, 2.2, and $3.7\,\mu m$ bands, respectively. With the exception of the $1.6\,\mu m$ band retrieval estimates, agreement is still excellent.

As another test of the weightings, consider clouds where effective radius *decreases* with height. While such a profile might be physically realizable in clouds containing drizzle, the current interest is mainly in checking the accuracy of the weightings when the more absorbing layers are located towards cloud base. This effectively increases photon penetration compared with an otherwise similar cloud having the larger radii at cloud top. Comparisons using the cloud models in Table 3a were repeated, but with the size profiles reversed from top to base. This is described by the identical profiles of Table 1, but with the original boundary conditions r_{base} and r_{top} switched. The adiabatic profile now decreases relatively slowly from cloud base upwards, with a rapid decrease near cloud top. Results are shown in Table 3b, where the w_m size estimate is now larger than the w_N^r estimate. Again, the w_m weighting estimate gives the best comparison with the retrievals, with overall differences similar to the previous results.

A further test of the w_m weighting arises when two separate cloud layers exist, such as a mid-level cloud overlying a stratus deck, each with significantly different droplet sizes. Ignoring absorption and scattering in the medium between the clouds, we can model the two layers as a single contiguous cloud with a discontinuity in the droplet size profile. This size discontinuity can provide a more demanding test of the weighting function, at least for bands where a significant part of the weighting is from the lower cloud layer. As an extreme case, consider two homogeneous clouds. Let R_1 be the reflectance in some band for the upper cloud alone, and R_c the net reflectance resulting from the superposition of both clouds. Then from Eq. 4, the net integrated weighting for the upper and lower cloud is R_1/R_c and $(R_c-R_1)/R_c=1-R_1/R_c$, respectively. Applying Eq. 3 therefore gives a weighting-inferred effective radius estimate of $r_e^{*}=r_{e1}(R_1/R_c)+r_{e2}(1-R_1/R_c)$, where r_{e1} and r_{e2} are the effective radii in the upper and lower cloud, respectively. For example, let $r_{e1}=10\,\mu m$, $r_{e2}=5\,\mu m$, $\tau_1=\tau_2=5$ (i.e., $\tau_c=10$), $\mu=0.85$, and $\mu_0=0.65$. The net weighting for the upper cloud is found to be 0.62, 0.68, and 0.92 for the 1.6, 2.2, and $3.7\,\mu m$ bands, respectively, giving size estimates of 8.1, 8.4, and $9.6\,\mu m$, respectively. The estimates for the two longer wavelength bands are found to be within $0.2\,\mu m$ of the retrievals (same analysis as Table 3), whereas the $1.6\,\mu m$ size estimate is about $0.8\,\mu m$ larger. As in Table 3, the $1.6\,\mu m$ band weighting estimate tends to differ most from the retrieval. This is due to the band's relatively weak droplet

absorption, and hence limited size information for clouds much thinner than that corresponding to the asymptotic reflectance limit.

We conclude that w_m provides an accurate, and apparently robust, weighting for use in Eq. 3. Further plots of this weighting are shown in Fig. 4 for visible and near-infrared bands and the cloud described in Fig. 2. The optical depth corresponding to the weighting-derived retrieved size is indicated on the plot. For the same cloud and solar zenith angle, Fig. 5a shows the weighting dependence on viewing angle for $0.45 \le \mu \le 0.95$, in each near-infrared band. The weighting for albedo is also shown. It is clear that larger viewing angles correspond to an increase in the upper cloud weighting. Retrieved sizes will therefore vary with both solar and viewing angles for inhomogeneous clouds. Table 4 gives the retrieved effective radius in each band as a function of viewing angle for the cloud of Fig. 5. Retrievals change by about $0.8\,\mu m$ in the shorter wavelength bands for $0.25 \le \mu \le 0.95$. The optical depth corresponding to the retrieved size is also given in the table along with the corresponding relative geometric depth $1-z/h$ (z is height from cloud base, h is total cloud geometric thickness). These depths are the level at which an in situ aircraft would have to fly to measure droplet sizes equivalent to the retrievals. The corresponding relative optical depth, τ/τ_c, ranges from less than 0.1 for the $3.7\,\mu m$ band at $\mu=0.25$, to over 0.5 for the $1.6\,\mu m$ band at a nadir view; similarly, relative geometric depth ranges from 0.05 to 0.4, respectively. Exchanging solar and viewing directions results in identical weightings, size estimates, and retrievals due to reciprocity in bidirectional reflectance as discussed previously. So the results of Fig. 5a and Table 4 are also valid for $\mu=0.65$ and μ_0 varying.

Two observations can be made. First, aircraft microphysical sampling at a single cloud level can give misleading validation results. Consider the adiabatic cloud example of Table 4 for $\mu=0.85$. An aircraft flying below cloud top at an altitude equal to one-third of the cloud geometric thickness, would measure an effective radius exactly equivalent to the $2.2\,\mu m$ band retrieval of $10.6\,\mu m$. The $1.6\,\mu m$ band retrieval is practically identical ($10.5\,\mu m$), also agreeing with the in situ measurement. However, the $3.7\,\mu m$ band retrieval would be $11.4\,\mu m$, or almost $1\,\mu m$ larger than the measured effective radius. The discrepancy would not be a fault of the retrieval, but an artifact of using in situ data from single level measurements in validating retrievals from a vertically inhomogeneous cloud. Of course, this discrepancy could increase or decrease significantly depending on the cloud optical thickness and droplet size profile. Droplet size measurements made at other cloud levels would differ from the 1.6 and $2.2\,\mu m$ band retrievals as well. As the viewing and/or solar zenith angle increases, the cloud level consistent with the retrievals moves towards cloud top. Therefore, a second observation is that for large zenith angles, it may be difficult to measure droplet sizes in the very upper regions of the cloud as needed for validation. This is especially true for comparison with 3.7 μm band retrievals where validation requires in situ measurements in the upper 10 % of the cloud for $\mu \leq 0.55$ (or μ_0).

5.1 Liquid Water Path Estimates

An estimate of liquid water path, *LWP*, can be made from optical thickness and effective radius retrievals. Combining Eqs. 1 and 2 while ignoring differences between the area-weighted, volume-weighted, and effective radius, yields $LWP \approx 2\tau r_e/3$, with effective radius in micrometers and liquid water path in $g m^{-2}$. The calculation is strictly valid only for homogeneous clouds having a constant droplet size at all levels. Previous results can be used to test the accuracy of the formulation for the inhomogeneous clouds of Table 2. Water path calculations are shown in Table 5 for the adiabatic cloud model, using size retrievals from Table 3a. Liquid water path retrievals generally overestimate actual water path since retrieved effective radii tend to be larger than the mean cloud droplet size. However, overestimates of the actual water path using 1.6 and 2.2 μm band retrievals is seen to be less than 10 %, and only about 5 % on average. The 3.7 μm band retrievals, having larger retrieved effective radii, overestimate water path by 5-17 %, and by about 12 % on average. As expected, the thicker clouds produce the larger errors. Use of the sub-adiabatic cloud model (profile *A*) results in smaller liquid water path retrieval errors than for adiabatic clouds. Cloud profile *D* retrievals tend to give largest water path errors with estimates being, on average, about 3 %, 9 %, and 20 % greater than actual for the 1.6, 2.2, and 3.7 μm band retrievals, respectively. In one case ($\tau_c=5$), the 1.6 μm band retrieval gives a water path less than the actual. However, as already discussed, profiles *A* and *B* are considered the most physically realistic profiles for single layer clouds, while profile *D* mainly serves to test the weighting formulations under more extreme circumstances. The results suggest that retrievals can provide reasonable estimates of liquid water paths, even for moderately thick vertically inhomogeneous clouds.

5.2 Comments on Transmittance-Inferred Retrievals

We have discussed the ability of the proposed weighting functions to predict reflectance-inferred size retrievals. Size retrievals can theoretically be made with

modeled transmittances in a manner similar to the reflectance-base retrievals of Table 3. However, transmittance measurements contain relatively little information regarding droplet size compared with reflectance measurements. This is due, in part, to the competing way in which droplet single scattering albedo and asymmetry parameter vary with effective radius as discussed in section 2. Two difficulties occur. First, the sensitivity of transmittance to effective radius over the expected droplet size range is much smaller than for reflectance. This a common difficulty to all the near-infrared bands. For example, $|dT/dr_e| \leq 0.005$ in the 2.2 μm band (for $\tau_c>1$, $r_e=8$ μm, $\mu=0.85$, $\mu_0=0.65$). In comparison, sensitivity for reflectance, dR/dr_e, is larger by a factor of 3 to 8 for the same situation. This implies that successful real-world transmittance retrievals would require much more accurate measurements and cloud models than reflectance retrievals. Secondly, and more problematic, transmittance curves do not always monotonically decrease with effective radius in the 1.6 and 2.2 μm bands. This can result in multiple solutions when attempting transmittance-inferred size retrievals. The problem does not appear to be as significant for the 3.7 μm band, though retrievals are now limited to relatively thin clouds due to the larger droplet absorption. Emission is also a source of difficulty in this band. So from a theoretical perspective, with no measurement or model error, we can at least test the effectiveness of the transmittance weighting w'_λ for the 3.7 μm band. The approach is identical to reflectance. For the thinnest cloud in Table 3a ($\tau_c=5$) the weighting gives size estimates within about 1 μm of the retrievals for both profiles, a greater discrepancy than for reflectance. The information content in transmittance measurements requires further study. However, for present purposes, the transmittance weighting calculation will still prove worthwhile in that the overall average number of scatterings can be used to estimate horizontal transport [*Platnick*, 1999a]. Figure 5b shows the transmittance weighting function, w'_λ, for the near-infrared bands as a function of viewing angle for the same cloud of Fig. 5a.

5.3 Retrievals in the Presence of a Reflecting Surface

Retrievals and weightings have been presented for clouds overlying a black surface. If downwelling intensity from cloud base can be considered Lambertian, the surface albedo of the ocean in visible and near-infrared bands is relatively small at about 0.04 (assuming that specular Fresnel reflectance is the main component, and ignoring surface roughness and sea foam). Land surface reflectances may vary widely for these bands [*Kaufman et al.*, 1997]. It is not obvious whether retrievals over a *known* reflecting surface will differ significantly from retrievals for the same cloud overlying a black surface. The assumption of the surface reflectance being known is very important. Error due to imperfect knowledge of the surface reflectance is not being investigated here, but rather the impact of the surface on the vertical weighting and size retrieval. It is expected that reflected photons having a scattering with the surface will increase the information contribution of lower layers and tend to reduce the retrieved effective radius (when droplet sizes increase with height). If the difference between retrievals with and without a known reflecting surface are negligible, then Eq. 4 is still directly applicable as a useful reflectance weighting. However, if the surface significantly modifies the retrieved cloud effective radius, r_e^*, then Eq. 3 implies that there must also be a noticeable change in the weighting. Calculations of both numerator and denominator in Eq. 4 can still be made in the presence of a reflecting surface. Though a maximum penetration interpretation would no longer be valid, the result may still yield a useful weighting.

Retrieval were made for the clouds of Table 3 overlying Lambertian surface reflectances of 0.20, 0.10, and 0.05 for the 1.6, 2.2, and 3.7 µm bands, respectively. The surface albedos are based on nominal values for measured vegetation scenes [*Kaufman et al.*, 1997]. As before, comparisons are made assuming the optical thickness is known exactly, eliminating specification of the visible surface albedo. In nearly all cases, retrievals changed insignificantly in the presence of the known reflecting surface (by less than 0.05 µm). The single exception was the 1.6 µm band retrieval for the cloud with τ_c=8, which showed a difference of about 0.2 µm for the linear profile (*L*); the adiabatic profile gave a smaller difference. This cloud model and band also proved problematic for the weighting estimates of Table 3. In general, relatively thick clouds will have enough absorption in the near infrared to effectively hide the surface from reflecting photons and consequently there can be no discernible change in the retrievals. Thinner clouds might allow the surface to have an impact on the weighting, but the relatively small changes in droplet size with height expected in a thin cloud should limit the impact on retrievals. Even a thin cloud, with a rather unlikely larger range in droplet size, can show little effect from the surface. For example, consider a cloud with τ_c=3, r_{base}=5 µm, r_{top}=10 µm (equivalent angles as in Table 3). Retrievals made with the reflecting surface were at most, 0.04 µm larger than retrievals made with the black surface, for all bands and profiles.

These examples suggest that the effect of a known surface reflectance on droplet size retrievals from vertically inhomogeneous clouds is negligible. If generally true,

calculations of w_m for a cloud overlying a black surface can still be used in estimating retrieved droplet sizes for clouds overlying vegetation.

5.4 Retrievals Based on Single Scattering

Details of the of the droplet phase function in the backscattered direction can be observed in the glory pattern. This is a single scattering phenomena where the difference in scattering angle between brightness peaks of the glory and/or the location of the peaks can be used to estimate droplet size [*Spinhirne and Nakajima*, 1994]. Similarly, polarization patterns observed with the POLDER instrument aboard the ADEOS satellite, also a single scattering method, have been used to infer cloud top droplet sizes [*Descloitres et al.*, 1998]. Due to the single scattering constraint, droplets contributing to either the glory or polarization pattern will be, on average, at a depth corresponding to the mean free optical path for scattered photons. By definition, the mean free path is an optical path of unity, and so representative droplets will be located at an optical depth of $(\mu^{-1}+\mu_0^{-1})^{-1}$ (accounting for slant path propagation). This can also be derived from either of the two weighting functions, w_m and w_N^{τ}, which are now equivalent for singly scattered photons. Following Eq. 4, the single scattering contribution to reflectance originating from a differential layer located at a depth τ can be written as $\mathrm{d}R(\tau) = \varpi_0 p(\Theta)\exp(-a\tau)\mathrm{d}\tau$, where $p(\Theta)$ is the scattering phase function at the scattering angle Θ, and $a=\mu^{-1}+\mu_0^{-1}$. The single scattering contribution from all differential layers between cloud top and the depth τ is found by integrating the last expression, assuming $p(\Theta)$ is constant over the vertical region where $\exp(-a\tau)$ is significant. The integration gives $R(\tau)=\varpi_0 p(\Theta)a^{-1}[1-\exp(-a\tau)]$. The denominator of Eq. 4, $R(\tau_c)$, then becomes $\varpi_0 p(\Theta)a^{-1}$ for a cloud optical thickness such that $a\tau_c \gg 1$, and the derivative in the numerator is evaluated as $\mathrm{d}R(\tau)/\mathrm{d}\tau = \varpi_0 p(\Theta)\exp(-a\tau)$. The ratio gives the weighting for single scattering as

$$w_{\mathrm{single}}(\tau) = a\, e^{-a\tau} \quad . \tag{5}$$

The average optical depth, $\bar{\tau}$, is given by the first moment of Eq. 5, which is a^{-1} as expected. Note that $\bar{\tau} \le 0.5$ (maximum for overhead solar and viewing angles). This close proximity to cloud top implies that single scattering retrieval methods will infer larger droplet sizes than the reflectance-inferred retrievals for adiabatic clouds, except in the optically thin limit where both are equivalent. As an example, optical depths corresponding to retrieved effective radii were given in Table 4 for the adiabatic cloud model with $\tau_c=8$. The table shows those depths to be much greater than the single scattering average depth for all bands, and at all viewing angles. For instance, the 2.2 μm band retrieval at $\mu=0.85$ and $\mu_0=0.65$ corresponds to a depth of 3.7 (effective radius of 10.6 μm), whereas the single scattering depth is 0.37 (effective radius of about 12 μm). However, cloud parcels this close to cloud top might be subject to significant entrainment from above. Regardless, it is practically difficult to get a statistically meaningful in situ measurement of droplet sizes this close to cloud top since an optical depth of 0.37 in this example implies a geometric depth of less than 10 m. Single scattering methods might therefore provide a practical method for studying cloud top microphysical processes.

5.5 Weighting Functions for Emission

Cloud thermal emission can be a significant, and sometimes dominant, part of the total measured intensity in the 3.7 μm band. For example, a uniform cloud that is optically thick at this wavelength ($\tau_c \approx 6$), with an effective radius of 10 μm and a temperature of 290 K, emits radiation that is roughly equivalent to the reflected solar radiation. Larger effective radii would have greater droplet absorption, thereby increasing cloud emissivity and emission, and decreasing cloud reflectance or transmittance. Reflectance-based retrieval algorithms compare the total upwelling 3.7 μm measured intensity with reflectance and emissivity libraries calculated from homogeneous cloud models. Because of differences in the source of the radiation, it is not obvious that emitted and solar reflected (or transmitted) radiation in vertically structured clouds would be represented by the same homogeneous cloud effective radius. Emission is further complicated by a potentially significant thermal structure. Analogous to the previous use of vertical weighting functions in solar scattering problems, we seek a function such that Eq. 3 approximates the effective radius of a homogeneous cloud having the same emission as the vertically inhomogeneous cloud. We denote this vertical weighting function as $w_e(\tau,\tau_c,\mu)$ corresponding to emission in the viewing direction μ. In general, for a vertically structured cloud, two separate weighting functions will be needed to describe emission transported to both cloud base and cloud top boundaries. In the following discussion, it is simpler to just use a single notation for both (unlike the use of superscripts in the solar weighting notation).

A straightforward candidate weighting for layer emission is one proportional the amount that a differential cloud layer contributes to the overall emitted intensity, i.e., a weighting defined such that $w_e(\tau,\tau_c,\mu)d\tau$ gives the radiation emerging at a cloud boundary in the direction μ, due to photons emitted in all directions from a layer of thickness $d\tau$, located at a depth τ, in a cloud of optical thickness τ_c. The normalization of this weighting is therefore the net cloud emission in the direction μ. The weighting is derived by first determining layer emission and then accounting for transport of layer emission to the boundaries. Radiation emitted by a differential cloud layer is $B(T)d\tau(1-\varpi_0)/\mu$, where $d\tau(1-\varpi_0)/\mu$ is the layer emissivity, $B(T)$ the Planck function, T the temperature of the differential layer, and ϖ_0 the layer's single scattering albedo. As usual, it is understood that all scattering and emission quantities are a function of wavelength as well as position within the vertically inhomogeneous cloud. Transport of layer emission to the cloud boundaries can be obtained from the escape operators, or escape matrices in the present numerical implementation. A discussion of escape operators in homogeneous emission problems and some examples are given in *Twomey* [1979]. Modifications to vertically inhomogeneous layers are straightforward.

For low-level adiabatic clouds, temperature decreases approximately linearly with height up to several kilometers in thickness. For a cloud 300 m thick (considered in Table 2), the temperature difference between cloud base and cloud top would only be a couple of degrees Kelvin. A sub-adiabatic cloud may be expected to have an even smaller lapse rate. In the 3.7 μm band, $\Delta T=2$ K corresponds to less than a 10% difference in the Planck function for warm clouds. For such cases, we can consider the clouds to be isothermal to first order. With $B(T)$ a constant, the proposed emission weighting reduces to the effective emissivity of the layer as observed from cloud top or base. Since $1-\varpi_0$ is approximately proportional to effective radius for cloud droplets in the near-infrared [*Twomey and Bohren*, 1980], replacing the weighting's $d\tau(1-\varpi_0)/\mu$ layer emissivity term with $d\tau/\mu$ would appear to give a weighting more appropriate for use in Eq. 3. The following examples suggest that this modification does help in describing cloud-top emission when modeled cloud effective radii decrease with height, but that the original weighting definition using layer emissivity works better when effective radii increase with height. This indicates that neither of the two weightings are exact in the sense of Eq. 3. Still, they provide an adequate approximation as demonstrated below.

Cloud-top vertical emission weightings for the 3.7 μm band were determined for four isothermal clouds with the vertical structure described in Table 2. The weightings were then used in Eq. 3 to approximate the effective radius of a homogeneous cloud having the same cloud-top emission as the vertically structured cloud. Results are summarized in Tables 6a for r_e increasing with height, when using the weighting proportional to layer emissivity. Table 6b gives results with r_e decreasing with height (equivalent to the cloud *base* emission weighting estimate when r_e increases with height) and using the modified weighting. These results can be compared with the droplet size inferred by matching calculations of homogeneous cloud-top emission for a range of effective radii, with the vertically structured cloud emission. This is analogous to a reflectance-based effective radius retrieval and is referred to in the table as the *emission-only retrieval*. Potential surface emission transmitted through the cloud is ignored. The weighting-derived effective radii are generally within several tenths of a micron of the retrieved size for the adiabatic clouds, and typically better than half a micron for clouds specified by effective radius linear with optical depth.

For comparison, Table 6 also gives reflection-inferred effective radius retrievals, referred to as *reflectance-only retrieval* (copied from Table 3). The very encouraging conclusion is that reflectance and emission-inferred effective radii retrievals for all modeled clouds are, on average, within 0.2 μm of each other and with a maximum difference of 0.4 μm; for the adiabatic cloud models, the maximum difference is 0.2 μm. For a homogeneous cloud, a single effective radius will of course correctly represent both cloud reflectance and emission. We have just seen that a consistent effective radius is likely to represent both reflectance and emission in vertically structured clouds as well. If this were not the case, retrieved radii would lie somewhere between the reflectance-inferred and emission-inferred size, depending on cloud temperature and structure. These results are somewhat remarkable given the difference in the emission and reflectance vertical weighting functions. An example is shown in Fig. 6. Despite the two weightings being significantly different, the weighting-derived effective radii are within 0.4 μm of each other.

Emission weighting function discussed in this section should also prove useful for studying cloud particle size retrievals using longer wavelengths, such as the 8.5, 10, and 11 μm bands [*Ackerman et al.*, 1998], and in comparing size information from those algorithms with solar scattering methods.

6. Information Regarding the Droplet Size Profile

To the extent that the retrieved effective radius varies with each near-infrared band in the examples of Table 3, there is evidently some information regarding the droplet size profile that may be inferred from the three retrievals. The weighting function plots of Fig. 5a also demonstrate that each near-infrared band is sampling the cloud layers in different proportions, suggesting the possibility of an inversion for the size profile. However, the relatively monotonic nature of the functions, except for a small maximum near cloud top, makes them less than optimum for inversions. A quantitative assessment of the information content in the three reflectance-based retrievals will be discussed in this section. It is the information content that is of immediate interest. Implementation and testing of an actual inversion algorithm is not undertaken. Ultimately, the usefulness and required accuracy of an inversion depends on the intended application (e.g., improvement in liquid water path estimates, cloud process studies, etc.).

At most, three pieces of unique information regarding the profile shape can be acquired from the three retrievals. However, both the figure and the retrieval results make it clear that there is relatively little difference in the informational content of the 1.6 and 2.2 μm bands compared with the 3.7 μm band. There will be an obvious difficulty in realizing unique information from both shorter wavelength bands when differences between the two retrievals are less than the retrieval uncertainty. For such a case, information is effectively limited to two pieces of information. Retrieval uncertainty can be present in the form of measurement error, error in weighting function effective radius estimates, and numerical error. The eigenvalues of the covariance, or correlation, matrix are a useful indication of the number of pieces of information provided by the three weightings in the presence of error. The elements of this symmetric matrix, $C_{i,j}$, are given by the inner product of the weightings (the weighting functions are equivalent to the kernels in inversion theory). For example, we can let $C_{1,2} = \int_0^{\tau_c} w_{1.6}(\tau,\tau_c)\, w_{2.2}(\tau,\tau_c)\, d\tau$, where the indices 1 and 2 refer to the 1.6 and 2.2 μm weightings, respectively. Likewise, index 3 will refer to the 3.7 μm band. It is useful to further normalize the retrieval equation (Eq. 3) by r_e^* which, in turn, scales the covariance matrix ($C_{i,j} \rightarrow C_{i,j}/r_{ei}^* r_{ej}^*$). Let e_r represents the relative error in retrieving r_e^* (assumed constant in all bands). Then for all weightings to contribute unique information, the minimum eigenvalue of the scaled covariance matrix must be greater than about e_r^2/Nr_m^2, where N is the number of measurements and r_m the mean value of the unknown $r_e(\tau)$ profile [*Twomey*, 1977].

As an example, consider the cloud specified by τ_c=8, r_{base}=5 µm, r_{top}=12 µm, with an adiabatic profile and geometry μ=0.85, μ_0=0.65 (retrievals given in Table 3). The value of r_m is about 10 µm for this cloud. Our own analysis suggests that it is doubtful that typical relative retrieval error can be expected to be better than 5 % in any band (due to limitations in cloud model library calculations and instrument uncertainty). Furthermore, the 1.6 µm band weighting function gave about 2.5 % error in the retrieval estimate for this cloud (Table 3a); weighting function error in the other bands were about 1 % or less. The combination of retrieval error and weighting function error suggests a minimum relative error in the range of 5-10 %. Therefore the minimum eigenvalues of the scaled covariance matrix need to be greater than about 8×10^{-6} to 3×10^{-5} for this example if each retrieval is to add information. It was found that the smallest eigenvalue (1×10^{-6}) is less than or equal to these limits while the other eigenvalues are larger, implying that only two pieces of information are available regarding the size profile. The 0.1 µm difference between 1.6 and 2.2 µm weighting-derived retrieval estimates (Tables 3a, 4) conveys the same conclusion. Some improvement can be had by using different viewing angles for each band, which is possible in low-level aircraft measurements. As shown in Fig. 5a, the peak in the weighting function moves toward cloud top and narrows as viewing zenith angle increases. The previous example was repeated with a viewing geometry of μ=0.95, 0.65, and 0.45 for the 1.6, 2.2, and 3.7 µm bands, respectively. After scaling , the eigenvalues are now 6.3×10^{-3}, 9.6×10^{-4}, and 3.2×10^{-5}. This implies that three pieces of information might be possible for 5 % relative error, but only two pieces can be expected for 10 % relative error. This is in accord with expectations from the retrievals results (Table 4), where the 1.6 and 2.2 µm retrieval size difference is 0.5 µm, or about 5 %. The analysis is for one particular case. Results will vary with cloud thickness, effective radius profile, and available geometry. However, similar conclusions occurred for other profiles and clouds from Table 2.

If three pieces of information are possible, it is not clear *which* three pieces are feasible. For instance, we could attempt to retrieve the three parameters a_0, a_1, and x in the analytic formula for the effective radius profile given in Table 1. As an alternative, $r_e(\tau)$ could be described by the three coefficients of a second-order polynomial. Though a quadratic is adequate for approximating profiles C and D of Fig. 1, a third-order polynomial is required to sufficiently approximate a typical adiabatic size profile. However, a quadratic form simplifies the quadrature of Eq. 3, giving the retrieved radius in any near-infrared band in terms of moments of the weighting function (i.e., $r_e^* = \alpha_0 + \alpha_1\bar{\tau} + \alpha_2\overline{\tau^2}$, where the α's are unknown coefficients of the quadratic fit, $\bar{\tau}$ is the first moment of $w_m(\tau,\tau_c)$, etc.). Retrieval estimates for the 1.6, 2.2, and 3.7 µm bands can then be expressed in matrix form by the rows of the equation $\boldsymbol{r_e^*} = \mathbf{A}\alpha$, where α is the unknown vector, $\boldsymbol{r_e^*}$ constitutes the measurement vector, and the matrix $\mathbf{A}$ contains the moments. Other profile retrieval alternatives include the effective radii in three layers of specified depth, or the effective radii in two layers of variable depth. If only two pieces of information are possible, a linear fit to the size profile might be retrieved (a physically unlikely profile as previously discussed) or alternatively, the effective radii in two layers of fixed depth.

Equation 3 for the weighting-derived retrieved droplet size estimate appears similar to a Fredholm integral of the first kind, an integral form which serves as a basis for a wide range of atmospheric inversion problems [*Twomey*, 1977]. However, the kernel in this equation is the maximum penetration weighting w_m which, though not explicitly indicated above, is also a function of the unknown profile $r_e(\tau)$. The resulting non-linearity between retrievals and the unknown precludes the use of a constrained linear inversion unless a linearized form of the equation, with a constant weighting function (e.g., derived from a nominal profile), proves satisfactory. Otherwise, an iterative approach is required.

In summary, the ability of three separate near-infrared band retrievals to infer three unique pieces of information regarding the droplet size profile is problematic at a fixed viewing angle (at least for the cloud example considered). It is likely that such an inversion would be limited to two pieces of information. The use of multiple viewing angles allows for the possibility of obtaining a third piece of information.

7. Discussion and Conclusions

Cloud optical thickness and microphysical remote sensing retrievals using solar measurements make use of information contained in a visible and near-infrared atmospheric window bands (at 1.6, 2.2, and 3.7 µm). The near-infrared bands have various amounts of absorption for water which increases with wavelength and cloud droplet size. Retrieval algorithms make use of cloud reflectance (possibly transmittance) look-up tables calculated from plane-parallel, homogeneous cloud models. The implication is that either observed clouds can be considered approximately homogeneous for retrieval purposes, i.e., vertical structure has little influence on effective radius retrievals, or else the retrieval is understood to be the plane-parallel, homogeneous equivalent value. If clouds are inhomogeneous, then separate near-infrared band retrievals may infer different effective radii, a situation which has been observed in airborne radiometer data [*Platnick et al.*, 1999]. We have relaxed the vertical homogeneity constraint in this paper and looked at the effect of modeled vertical droplet size profiles on retrieved effective radii.

Modeled effective radius profiles were developed for clouds which are sub-adiabatic at upper levels, adiabatic clouds, and two cloud models with drying at midlevels. For adiabatic clouds, absolute differences between 1.6 and 2.2 μm retrievals are typically half a micrometer or less, about the same size as the minimum expected retrieval error; 3.7 μm retrievals may be larger than for either of the other two bands (almost one micrometer for the adiabatic cloud models considered). Clouds with midlevel drying had the largest differences, up to one micrometer between 1.6 and 2.2 μm band retrievals, and over 1.5 μm differences between 2.2 and 3.7 μm band retrievals. All retrievals were made assuming that the cloud optical thickness was known without error, despite there being some coupling between size and thickness retrievals, especially for the 1.6 μm band. Retrievals provided reasonably good liquid water path estimates for adiabatic clouds, overestimating by about 5% on average for 1.6 and 2.2 μm retrievals and 12% for 3.7 μm retrievals. The maximum cloud optical thickness being modeled was 15, and water path error will increase with optical thickness (all else being equal). The midlevel drying cloud models caused overestimates of 10 to 20% in the 2.2 and 3.7 μm retrievals. In summary, adiabatic cloud retrievals showed relatively minor influences due to the vertical structure of cloud droplet effective radius. Clouds which are sub-adiabatic at upper levels give retrieval results that are even more homogeneous-like. Multilayer cloud systems are likely to have the most significant retrieval signatures.

Several vertical weighting functions were proposed for approximating the retrieved size. The most accurate weighting for reflection retrievals was one based on maximum photon penetration. This weighting was able to predict retrieved radii from the various vertically inhomogeneous cloud models to within a tenth of a micrometer for the 2.2 and 3.7 μm bands, and within a third of a micrometer for the less absorbing 1.6 μm band. Retrievals from glory or polarization single-scattering reflectance patterns infer droplet sizes from the very uppermost region of the cloud (within meters of cloud top), and thus may be substantially different from total reflectance retrievals (dominated by multiple scattering). For the same reason, single scattering retrievals would be difficult, if not impossible, to validate. In addition to providing information regarding the scale of

vertical transport, the weightings provide a means for investigating and understanding the possibility of an inversion for the droplet size profile using the three near-infrared size retrievals. Analysis shows that the most likely possibility for realizing three unique pieces of information from the retrievals is through the use of multiple viewing angles.

Though the emphasis of this work has been on multiple scattering weighting functions for liquid water clouds, the derived techniques should be applicable to any multiple scattering plane-parallel radiative transfer problem, including arbitrary combinations of cloud (liquid or ice particles), aerosol, and gas layers.

Acknowledgments. This work was supported in part by grant NAG5-6996 from the National Aeronautics and Space Administration, EOS validation program office. The author wishes to thank D. Flittner, R. Pincus, and S. Twomey for helpful discussions.

References

Ackerman, S.A., C.C. Moeller, K.I. Strabala, H.E. Gerber, L.E. Gumley, W.P. Menzel, and S.C. Tsay, Retrieval of effective microphysical properties of clouds: A wave cloud case study, *Geophys. Res. Lett.*, *25*, 1121-1124, 1998.

Ackerman, S.A., W.L. Smith, A.D. Collard, X.L. Ma, H.E. Revercomb, and R.O. Knuteson, Cirrus cloud properties derived from high spectral resolution infrared spectrometry during FIRE II. Part II: Aircraft HIS results, *J. Atmos. Sci.*, *52*, 4246-4263, 1995.

Albrecht, B.A., Aerosols, Cloud Microphysics, and Fractional Cloudiness, *Science*, *245*, 1227-1230, 1989.

Arking, A., and J.D. Childs, Retrieval of cloud cover parameters from multispectral satellite images, *J. Climate Appl. Meteor.*, *24*, 322-333, 1985.

Austin, P., Y. Wang, R. Pincus, and V. Kujala, Precipitation in stratocumulus clouds: observational and modeling results, *J. Atmos. Sci.*, *52*, 2329-2352, 1995.

Cahalan, R.F., and J.B. Snider, Marine stratocumulus structure, *Remote Sens. Environ.*, *28*, 1989.

Chandrasekhar, S., *Radiative Transfer*, 393 pp., Dover Publications, Inc., New York, 1960.

Charlson, R.J., J.E. Lovelock, M.O. Andreae, and S.G. Warren, Oceanic Phytoplankton, Atmospheric Sulfur, Cloud Albedo and Climate, *Nature*, *326*, 655-661, 1987.

Curry, J.A., Interactions among turbulence, radiation, and microphysics in arctic stratus clouds, *J. Atmos. Sci.*, *43*, 90-106, 1986.

Descloitres, J., J.C. Buriez, F. Parol, and Y. Fouquart, POLDER observations of cloud bidirectional reflectances compared to a plane-parallel model using the International Satellite Cloud Climatology Project cloud phase function, *J. Geophys. Res.*, *103*, 11411-11418, 1998.

Foot, J.S., Some observations of the optical properties of cloud. Part I: Stratocumulus., *Quart. J. Roy. Meteor. Soc.*, *114*, 129-144, 1988.

Garrett, T.J., and P.V. Hobbs, Long-range transport of continental aerosols over the Atlantic Ocean and their effects on cloud structure, *J. Atmos. Sci.*, *52*, 2977-2984, 1995.

Gerber, H., B.G. Arends, and A.S. Ackerman, New microphysics sensor for aircraft use, *Atmos. Res.*, *31*, 235-252, 1994.

Han, Q., W. Rossow, R. Welch, A. White, and J. Chou, Validation of satellite retrievals of cloud microphysics and liquid water path using observations from FIRE, *J. Atmos. Sci.*, *52*, 4183-4195, 1995.

Han, Q., W.B. Rossow, and A.A. Lacis, Near-global survey of effective droplet radii in liquid water clouds using ISCCP data, *J. Climate*, *7*, 465-497, 1994.

Kaufman, Y.J., A.E. Wald, L.A. Remer, B.-C. Gao, R.-R. Li, and L. Flynn, The MODIS 2.1-μm channel - correlation with visible reflectance for use in remote sensing of aerosol, *IEEE Trans. Geosci. Remote Sensing*, *35*, 1286-1298, 1997.

Kiehl, J.T., Sensitivity of a GCM Climate Simulation to Differences in Continental Versus Maritime Cloud Drop Size, *J. Geophys. Res.*, *99*, 23107-23115, 1994.

King, M.D., Y.J. Kaufman, W.P. Menzel, and D. Tanre, Remote-Sensing of Cloud, Aerosol, and Water-Vapor Properties From the Moderate Resolution Imaging Spectrometer (Modis), *IEEE Trans. Geosci. Remote Sensing*, *30*, 2-27, 1992.

Martin, G.M., D.W. Johnson, and A. Spice, The measurement and parameterization of effective radius of droplets in warm stratocumulus clouds, *J. Atmos. Sci.*, *51*, 1823-1842, 1994.

McFarquhar, G.M., and A.J. Heymsfield, The definition and significance of an effective radius for ice clouds, *J. Atmos. Sci.*, *55*, 2039-2052, 1998.

Nakajima, T., and M.D. King, Determination of the optical thickness and effective particle radius of clouds from reflected solar radiation measurements. I. Theory, *J. Atmos. Sci.*, *47*, 1878-1893, 1990.

Nakajima, T., M.D. King, J.D. Spinhirne, and L.F. Radke, Determination of the optical thickness and effective particle radius of clouds from reflected solar radiation measurements. II. Marine stratocumulus observations, *J. Atmos. Sci.*, *48*, 728-750, 1991.

Nicholls, S., and J. Leighton, An observational study of the structure of stratiform cloud sheets: Part I. Structure, *Quart. J. Roy. Meteor. Soc.*, *112*, 431-460, 1986.

Noonkester, V.R., Droplet spectra observed in marine stratus cloud layers, *J. Atmos. Sci.*, *41*, 829-845, 1984.

Ou, S.C., K.N. Liou, Y. Takano, N.X. Rao, Q. Fu, A.J. Heymsfield, L.M. Miloshevich, B. Baum, and S.A. Kinne, Remote sounding of cirrus cloud optical depths and ice crystal sizes from AVHRR data: Verification using FIRE II IFO measurements, *J. Atmos. Sci.*, *52*, 4143-4158, 1995.

Parol, F., J.C. Buriez, g. Brogniez, and Y. Fouquart, Information content of AVHRR channels 4 and 5 with respect to the effective radius of cirrus cloud particles, *J. Appl. Meteor.*, *30*, 973-984, 1991.

Pincus, R., and M.B. Baker, Effect of precipitation on the albedo susceptibility of clouds in the marine boundary layer, *Nature*, *372*, 250-252, 1994.

Platnick, S., The scales of photon transport in cloud remote sensing problems, in *International Radiation Symposium: Current Problems in Atmospheric Radiation*, edited by W. L. Smith, and K. Stamnes, pp. 206-209, A. Deepak Publishing, Fairbanks, AK, 1996.

Platnick, S., Approximations for horizontal photon transport in cloud remote sensing problems, *J. Quant. Spectrosc. Radiat. Transfer* (submitted), 1999a.

Platnick, S., A superposition technique for deriving photon scattering statistics in plane-parallel cloudy atmospheres, *J. Quant. Spectrosc. Radiat. Transfer* (submitted), 1999b.

Platnick, S., P.A. Durkee, K. Nielsen, J.P. Taylor, S.-C. Tsay, M.D. King, R.J. Ferek, P.V. Hobbs, and J.W. Rottman, The role of background cloud microphysics in the radiative formation of ship tracks, *J. Atmos. Sci.*, *In press*, 1999.

Platnick, S., and S. Twomey, Determining the susceptibility of cloud albedo to changes in droplet concentrations with the Advanced Very High Resolution Radiometer, *J. Appl. Meteor.*, *33*, 334-347, 1994.

Platnick, S., and F.P.J. Valero, A validation of a satellite cloud retrieval during ASTEX, *J. Atmos. Sci.*, *52*, 2985-3001, 1995.

Rawlins, F., and J.S. Foot, Remotely sensed measurements of stratocumulus properties during FIRE using the C130 aircraft multi-channel radiometer, *J. Atmos. Sci.*, *47*, 2488-2503, 1990.

Slingo, A., Sensitivity of the Earth's Radiation Budget to Changes in Low Clouds, *Nature*, *343*, 49-51, 1990.

Slingo, A., S. Nicholls, and J. Schmetz, Aircraft observations of marine stratocumulus during JASIN, *Quart. J. Roy. Meteor. Soc.*, 833-856, 1982.

Spinhirne, J.D., and T. Nakajima, Glory of Clouds in the Near-Infrared, *Appl. Opt.*, *33*, 4652-4662, 1994.

Stephens, G.L., and C.M.R. Platt, Aircraft observations of the radiative and microphysical properties of stratocumulus and cumulus cloud fields, *J. Climate Appl. Meteor.*, *26*, 1243-1269, 1987.

Twomey, S., Pollution and the planetary albedo, *Atmos. Environ.*, *8*, 1251-1256, 1974.

Twomey, S., *Introduction to the mathematics of inversion in remote sensing and indirect measurements*, 243 pp., Dover Publications, Inc., Mineola, NY, 1977.

Twomey, S., Doubling and superposition methods in the presence of thermal emission, *J. Quant. Spectrosc. Radiat. Transfer*, *22*, 355-363, 1979.

Twomey, S., Aerosols, clouds, and radiation, *Atmos. Environ.*, *25A*, 2435-2442, 1991.

Twomey, S., and C.F. Bohren, Simple approximations for calculations of absorption in clouds, *J. Atmos. Sci.*, *37*, 2086-2094, 1980.

Twomey, S., and T. Cocks, Spectral reflectance of clouds in the near-infrared: Comparison of measurements and calculations, *J. Meteor. Soc. Japan*, *60*, 583-192, 1982.

Twomey, S., and T. Cocks, Remote sensing of cloud parameters from spectral reflectance measurements in the near-infrared, *Beitr. Phys. Atmos.*, *62*, 172-179, 1989.

Twomey, S., H. Jacobowitz, and H.B. Howell, Matrix methods for multiple scattering problems, *J. Atmos. Sci.*, *23*, 101-108, 1966.

Wielicki, B.A., R.D. Cess, M.D. King, D.A. Randall, and E.F. Harrison, Mission to Planet Earth - Role of Clouds and Radiation in Climate, *Bull. Amer. Meteor. Soc.*, *76*, 2125-2153, 1995.

Young, D.F., P. Minnis, D. Baumgardner, and H. Gerber, Comparison of in situ and satellite-derived cloud properties during SUCCESS, *Geophys. Res. Lett.*, *25*, 1125-1128, 1998.

List of Figures

Fig. 1 Example of the four analytic models for the vertical profile of effective radius, r_e, considered in Table 1 for the *same* prescribed boundary conditions (total cloud optical thickness, τ_c, is 8 and effective radius is 5 µm and 12 µm at cloud base and top, respectively). The top plot shows effective radius as a function of optical depth, τ. The bottom two plots show the corresponding profile of r_e and cloud liquid water content, LWC, as a function of geometric height z, where h is the total thickness. The constraints used in deriving the profiles are indicated along side each plot. Note that for an otherwise identical cloud processes, cloud top r_e and LWC would be smaller for the sub-adiabatic profile (shown for x=0.75).

Fig. 2. Two proposed normalized vertical weighting functions, w_m (proportional to maximum photon penetration) and w_N (proportional to number of photon scatterings), for a 2.2 µm channel, using both superposition formulae (lines) and Monte Carlo calculations (symbols). Calculated for a cloud with a total optical thickness of 8, effective radius varying from 5 µm at cloud base to 12 µm at cloud top with profile C in Table 1, cosine of solar zenith and viewing angles of μ_0=0.65 and μ=0.85, respectively, and an azimuthal average. Plots of the scattering-based weighting function include weightings for both reflected and transmitted photons, w_N^r and w_N^t, respectively.

Fig. 3. The dependence of the normalized vertical weighting functions on cloud optical thickness, τ_c, for reflectance(top plot) and transmittance (bottom), for a 2.2 µm channel. For effective radius varying from 5 µm at cloud base to 12 µm at cloud top with profile C in Table 1, cosine of solar zenith and viewing angles of μ_0=0.65 and μ=0.85, respectively, and an azimuthal average.

Fig. 4. Normalized vertical weighting w_m for bidirectional reflectance, for visible and near-infrared cloud remote sensing channels, calculated using the superposition formulae discussed in the text, and the cloud described in Fig. 2. The cloud optical depth corresponding to the retrieved radii for each near-infrared channel is also indicated.

Fig. 5a. The dependence of the normalized bidirectional reflectance weighting w_m on the cosine of the viewing angle, μ, for the three near-infrared channels, and the cloud described in Fig. 2. The weighting for reflected flux, or albedo, is also shown.

Fig. 5b. Same as Fig. 4a, but for the bidirectional and flux transmittance weighting function w_N^t.

Fig. 6. Example of normalized reflectance and emissivity weightings for a 3.7 µm channel. Calculated for a cloud with a total optical thickness of 8, effective radius varying as from 5 µm at cloud base to 12 µm at cloud top with profile C in Table 1, cosine of solar zenith and viewing angles of μ_0=0.65 and μ=0.85, respectively, and an azimuthal average. Though the curves are significantly different, the weighting-derived effective radii (Eq. 3) differ by only a few tenths of a micron for the profile chosen.

Table 1. Analytic models for the vertical structure of effective radius, r_e, and liquid water content, LWC, versus geometric cloud height, z, and optical depth, τ. The following convention is used: z increases with height with $z=0$ at cloud base to $z=h$ at cloud top; optical depth increases towards cloud base with $\tau=0$ at cloud top; τ_c is the total cloud optical thickness. The constants a_0, a_1 are found from the optical thickness and the prescribed boundary conditions for droplet size at cloud top and base, r_{top} and r_{base}, respectively. Other constants (b, c) can be found in a similar manner.

Vertical Structure				
$LWC(z)$	$r_e(z)$	$r_e(\tau)$	a_0	a_1
$\left(c_0 + c_1 \frac{z}{h}\right)^x$	$\left(b_0 + b_1 \frac{z}{h}\right)^{\frac{x}{3}}$	$\left(a_0 - a_1 \frac{\tau}{\tau_c}\right)^{\frac{x}{2x+3}}$	$r_{top}^{\frac{2x+3}{x}}$	$r_{top}^{\frac{2x+3}{x}} - r_{base}^{\frac{2x+3}{x}}$

Profile	**Constraint**	x	**Physical Implication**
A	sub-adiabatic aloft	$0 < x < 1$	increasing entrainment/drying towards cloud top
B	$LWC(z) \sim z$	1	adiabatic
C	$r_e(z) \sim z$	3	sub-adiabatic at mid levels
D	$r_e(\tau) \sim \tau$	-3	sub-adiabatic at mid levels (useful test of weighting formulations)

Table 2. Two analytic profiles for the functional dependence of effective radius on cloud optical depth (see Table 1) and resulting microphysics. *LWP* is cloud liquid water path, *LWC* is liquid water content, N is droplet number concentration (assumed constant with height), and h is cloud geometrical thickness. The wavelength-independent optical thickness entry is for a scaled optical path using an extinction efficiency of $Q_e = 2.0$; *LWP* is calculated using the actual optical thickness for a 0.66 µm channel ($Q_e \approx 2.08 - 2.20$, depending on effective radius). Clouds are built up from homogeneous layers with scaled optical thicknesses of 0.25 and integer effective radii closest to the value given by the analytic formulas evaluated at the midpoint of the layer. Shaded entries give example microphysics for $h = 0.3$ km.

Cloud specifications		*Vertical structure*							
		profile D				profile B (adiabatic)			
τ_c	r_e cloud base-top (µm)	*LWP* (g m^{-2})	$N h$ (cm^{-3} km)	N for h=0.3 km (cm^{-3})	*LWC* of base, top layer for h=0.3 km (g m^{-3})	*LWP* (g m^{-2})	$N h$ (cm^{-3} km)	N for h=0.3 km (cm^{-3})	*LWC* of base, top layer for h=0.3 km (g m^{-3})
15	4–10	75	60.6	202	0.05, 0.85	89	37.0	123	0.06, 0.52
10	6–15	74	17.8	59	0.05, 0.84	88	11.1	37	0.05, 0.52
8	5–12	48	21.3	71	0.04, 0.51	57	13.8	46	0.04, 0.33
5	8–12	35	8.2	27	0.06, 0.20	37	7.5	25	0.05, 0.18

Table 3a. Comparison of reflectance-inferred effective radius retrievals with estimates obtained from two different vertical weightings, w_m and w_N^r, using Eq. 3. The effective radius retrieval gives the droplet size of a homogeneous cloud having a bidirectional reflectance equivalent to that of the vertically structured cloud. Calculations are for horizontally homogeneous plane-parallel cloud layers with effective radii *increasing* towards cloud top. Two analytic profiles for the functional dependence of effective radius on cloud optical depth are considered (see Table 2). The total cloud optical thickness, τ_c, is assumed to be known exactly when determining both the weighting-derived effective radius and the reflectance-inferred retrieval. Comparisons are for bidirectional reflectance with cosine of the solar and viewing zenith angles of μ_0=0.65, μ=0.85, and an azimuthal average. Calculations are for a black surface at all wavelengths.

Cloud specifications			*Vertical structure*					
			profile D			profile B (adiabatic)		
τ_c	λ (µm)	r_e cloud base-top (µm)	r_e^* retrieval (µm)	r_e^* w_m estimate (µm)	r_e^* w_N^r estimate (µm)	r_e^* retrieval (µm)	r_e^* w_m estimate (µm)	r_e^* w_N^r estimate (µm)
15	1.6	4–10	7.3	7.9	8.1	8.8	9.1	9.3
	2.2		8.1	8.3	8.4	9.3	9.3	9.4
	3.7		9.4	9.3	9.3	9.9	9.9	9.9
10	1.6	6–15	10.8	11.3	12.0	13.0	13.2	13.7
	2.2		11.8	11.7	12.2	13.6	13.5	13.9
	3.7		13.4	13.3	13.3	14.5	14.4	14.5
8	1.6	5–12	8.0	8.9	9.6	10.2	10.5	10.9
	2.2		9.1	9.1	9.7	10.7	10.6	11.0
	3.7		10.5	10.3	10.4	11.4	11.4	11.4
5	1.6	8–12	10.0	10.2	10.6	10.4	10.6	11.0
	2.2		10.3	10.3	10.7	10.7	10.7	11.0
	3.7		10.9	10.8	11.0	11.2	11.1	11.3

Table 3b. Same as Table 3a, but for plane-parallel cloud layers with effective radii *decreasing* towards cloud top.

Cloud specifications τ_c	λ (μm)	r_e cloud base-top (μm)	*Vertical structure* profile *D* r_e^* retrieval (μm)	profile *D* r_e^* w_m estimate (μm)	profile *D* r_e^* w_N^r estimate (μm)	profile *B* (adiabatic) r_e^* retrieval (μm)	profile *B* (adiabatic) r_e^* w_m estimate (μm)	profile *B* (adiabatic) r_e^* w_N^r estimate (μm)
15	1.6	10–4	6.0	5.7	5.6	4.5	4.3	4.2
	2.2		5.6	5.4	5.3	4.2	4.2	4.2
	3.7		4.8	4.7	4.6	4.0	4.0	4.0
10	1.6	15–6	9.2	9.2	8.7	6.9	6.8	6.5
	2.2		8.6	8.7	8.4	6.6	6.6	6.4
	3.7		7.5	7.4	7.3	6.2	6.2	6.1
8	1.6	12–5	7.5	7.7	7.2	5.8	5.7	5.4
	2.2		7.2	7.3	7.0	5.6	5.5	5.4
	3.7		6.5	6.4	6.2	5.2	5.2	5.2
5	1.6	12–8	9.8	9.9	9.5	9.2	9.1	8.7
	2.2		9.7	9.8	9.5	8.9	9.0	8.7
	3.7		9.2	9.2	9.1	8.5	8.5	8.4

Table 4. Weighting-derived effective radius retrieval versus cosine of the viewing zenith angle, μ. Calculated for $\tau_c = 8$, effective radii varying from $r_{base} = 5$ μm to $r_{top} = 12$ μm with an adiabatic profile, and $\mu_0 = 0.65$.

Viewing zenith angle μ	1.6 μm r_e^* w_m estimate (μm)	1.6 μm τ corresponding to r_e^*	1.6 μm 1- z/h corresponding to r_e^*	2.2 μm r_e^* w_m estimate (μm)	2.2 μm τ corresponding to r_e^*	2.2 μm 1- z/h corresponding to r_e^*	3.7 μm r_e^* w_m estimate (μm)	3.7 μm τ corresponding to r_e^*	3.7 μm 1- z/h corresponding to r_e^*
0.95	10.4	4.2	0.38	10.6	3.8	0.34	11.3	2.2	0.19
0.85	10.5	4.0	0.36	10.6	3.7	0.33	11.4	1.9	0.16
0.75	10.6	3.8	0.34	10.8	3.4	0.30	11.5	1.7	0.14
0.65	10.7	3.5	0.32	10.9	3.1	0.28	11.5	1.5	0.12
0.55	10.8	3.3	0.29	11.0	2.9	0.25	11.6	1.3	0.10
0.45	11.0	3.0	0.26	11.1	2.5	0.22	11.7	1.1	0.09
0.35	11.1	2.6	0.23	11.3	2.2	0.19	11.8	0.8	0.07
0.25	11.2	2.3	0.19	11.4	1.9	0.15	11.8	0.6	0.05
0.15	11.4	1.9	0.16	11.5	1.5	0.12	11.9	0.4	0.04

Table 5. Comparison of reflectance-inferred liquid water path (LWP) with the actual water path. Calculations are for horizontally homogeneous plane-parallel cloud layers with effective radii *increasing* towards cloud top. Two analytic possibilities for the functional dependence of effective radius on cloud optical depth are considered (see Table 2). The total cloud optical thickness, τ_c, is assumed to be known exactly when determining the retrieved effective radius. Comparisons are for bidirectional reflectance with $\mu_0=0.65$, $\mu=0.85$, and an azimuthal average. Calculations are for a black surface at all wavelengths.

Cloud specifications			*Vertical structure* profile *B* (adiabatic)		
τ_c	λ (µm)	r_e cloud base-top (µm)	r_e^* retrieval (µm)	LWP retrieval/actual	LWP actual (g m^{-3})
15	1.6	4–10	8.8	1.06	
	2.2		9.3	1.10	89
	3.7		9.9	1.17	
10	1.6	6–15	13.0	1.03	
	2.2		13.6	1.08	88
	3.7		14.5	1.15	
8	1.6	5–12	10.2	1.00	
	2.2		10.7	1.05	57
	3.7		11.4	1.12	
5	1.6	8–12	10.4	1.00	
	2.2		10.7	1.03	37
	3.7		11.2	1.05	

Table 6a. Comparison of 3.7 µm reflectance-inferred effective radius retrievals with that of emission for an isothermal cloud. The effective radius retrieval corresponding to reflectance is the droplet size of a homogeneous cloud giving a bidirectional reflectance equivalent to that of the vertically structured cloud. The effective radius retrieval corresponding to emission is the droplet size of a homogeneous cloud giving an emissivity equivalent to that of the vertically structured cloud; an estimate of this radius using an emission weighting, w_e, proportional to $(1-\varpi_0)d\tau/\mu_i$, with Eq. 3 is also shown. Calculations are for horizontally homogeneous plane-parallel cloud layers with effective radii *increasing* towards cloud top. The total cloud optical thickness, τ_c, is assumed to be known exactly. Comparisons are for $\mu_0=0.65$, $\mu=0.85$, an azimuthal average, and a black surface.

Cloud specifications			*Vertical structure* profile *D*			profile *B* (adiabatic)		
τ_c	λ (µm)	r_e cloud base-top (µm)	r_e^* reflectance-only retrieval (µm)	r_e^* emission-only retrieval (µm)	r_e^* w_e estimate (µm)	r_e^* reflectance-only retrieval (µm)	r_e^* emission-only retrieval (µm)	r_e^* w_e estimate (µm)
15	3.7	4–10	9.4	9.1	8.7	9.9	9.8	9.6
10	3.7	6–15	13.4	13.0	12.5	14.5	14.2	13.9
8	3.7	5–12	10.5	10.1	9.8	11.4	11.2	11.0
5	3.7	8–12	10.9	10.8	10.6	11.2	11.1	10.9

Table 6b. Same as Table 6a, but for plane-parallel cloud layers with effective radii *decreasing* towards cloud top, and an emission weighting, w_e, proportional to $d\tau/\mu_i$.

Cloud specifications			*Vertical structure*					
			profile *D*			profile *B* (adiabatic)		
τ_c	λ (μm)	r_e cloud base-top (μm)	r_e^* reflectance-only retrieval (μm)	r_e^* emission-only retrieval (μm)	r_e^* w_e estimate (μm)	r_e^* reflectance-only retrieval (μm)	r_e^* emission-only retrieval (μm)	r_e^* w_e estimate (μm)
15	3.7	10–4	4.8	5.1	5.2	4.0	4.2	4.2
10	3.7	15–6	7.5	7.6	8.4	6.2	6.3	6.5
8	3.7	12–5	6.5	6.8	7.1	5.2	5.4	5.5
5	3.7	12–8	9.2	9.4	9.6	8.5	8.6	8.8

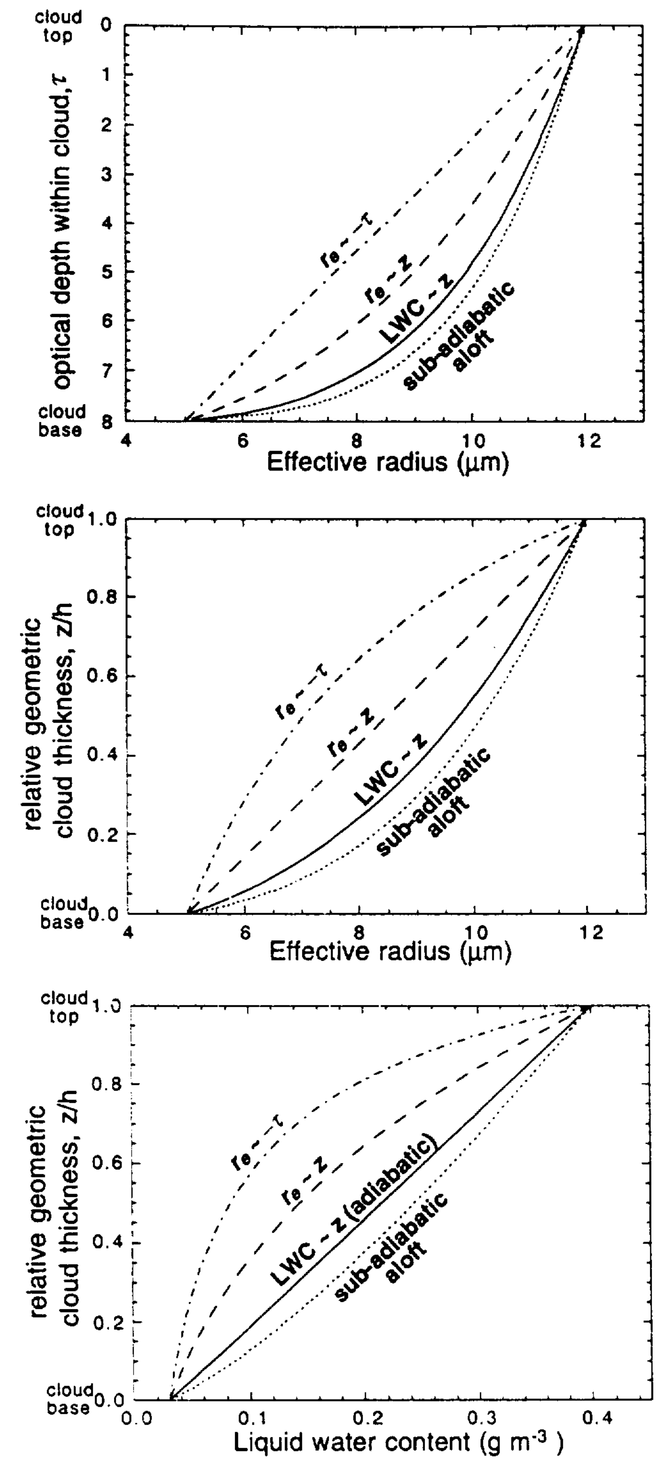

Fig. 1. Example of the four analytic models for the vertical profile of effective radius, r_e, considered in Table 1 for the *same* prescribed boundary conditions (total cloud optical thickness, τ_c, is 8 and effective radius is 5 μm and 12 μm at cloud base and top, respectively). The top plot shows effective radius as a function of optical depth, τ. The bottom two plots show the corresponding profile of r_e and cloud liquid water content, *LWC*, as a function of geometric height z, where h is the total thickness. The constraints used in deriving the profiles are indicated along side each plot. Note that for an otherwise identical cloud processes, cloud top r_e and *LWC* would be smaller for the sub-adiabatic profile (shown for x=0.75).

Platnick

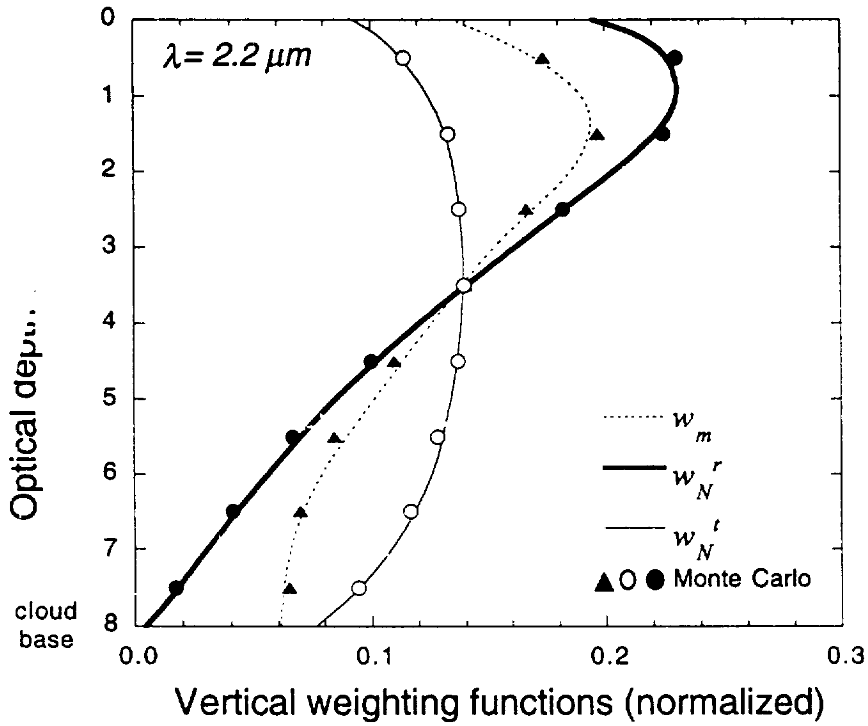

Fig. 2. Two proposed normalized vertical weighting functions, w_m (proportional to maximum photon penetration) and w_N (proportional to number of photon scatterings), for a 2.2 μm channel, using both superposition formulae (lines) and Monte Carlo calculations (symbols). Calculated for a cloud with a total optical thickness of 8, effective radius varying from 5 μm at cloud base to 12 μm at cloud top with profile *C* in Table 1, cosine of solar zenith and viewing angles of μ_0=0.65 and μ=0.85, respectively, and an azimuthal average. Plots of the scattering-based weighting function include weightings for both reflected and transmitted photons, w_N^r and w_N^t, respectively.

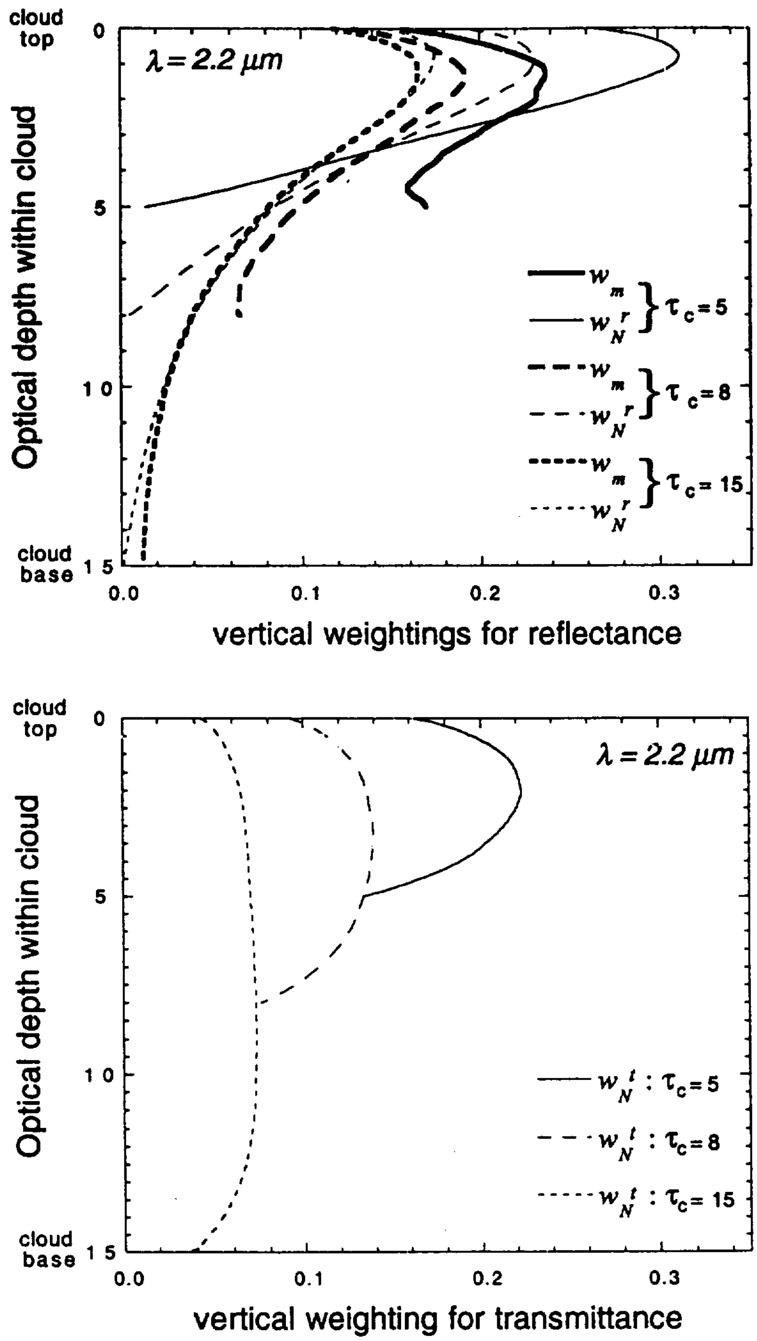

Fig. 3. The dependence of the normalized vertical weighting functions on cloud optical thickness, τ_c, for reflectance(top plot) and transmittance (bottom), for a 2.2 μm channel. For effective radius varying from 5 μm at cloud base to 12 μm at cloud top with profile *C* in Table 1, cosine of solar zenith and viewing angles of μ_0=0.65 and μ=0.85, respectively, and an azimuthal average.

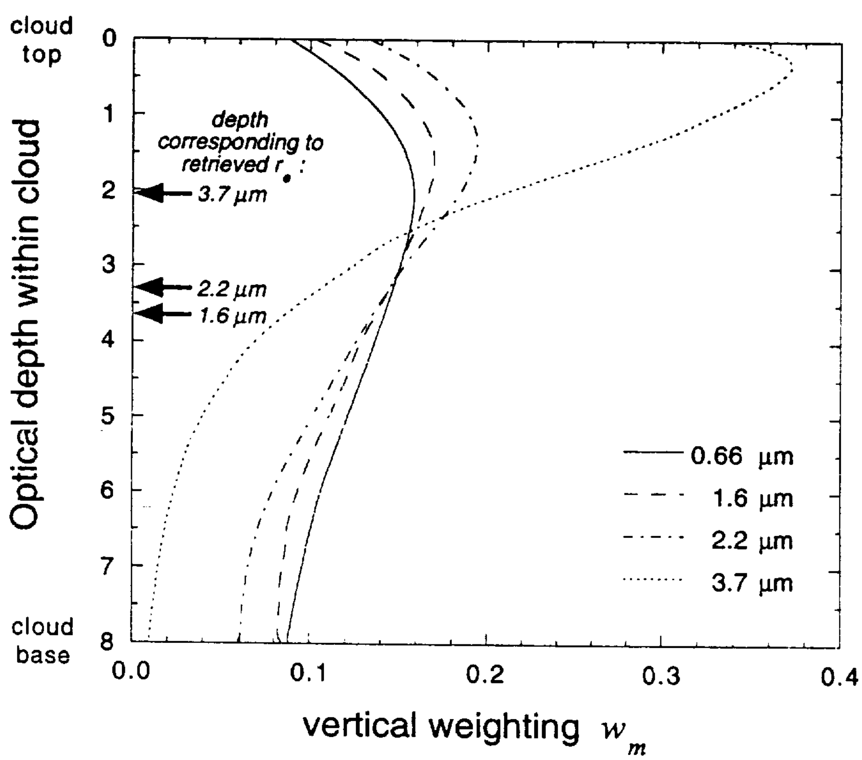

Fig. 4. Normalized vertical weighting w_m for bidirectional reflectance, for visible and near-infrared cloud remote sensing channels, calculated using the superposition formulae discussed in the text, and the cloud described in Fig. 2. The cloud optical depth corresponding to the retrieved radii for each near-infrared channel is also indicated.

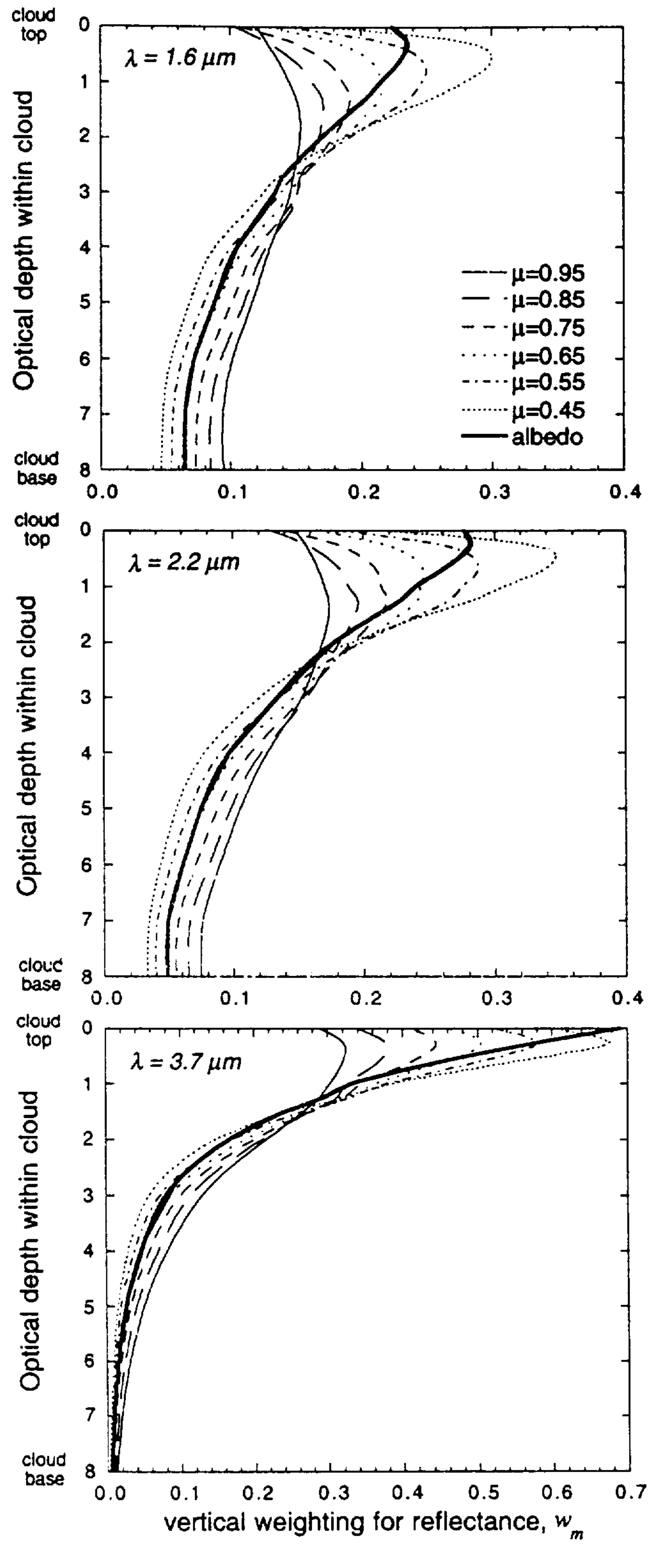

Fig. 5a. The dependence of the normalized bidirectional reflectance weighting w_m on the cosine of the viewing angle, μ, for the three near-infrared channels, and the cloud described in Fig. 2. The weighting for reflected flux, or albedo, is also shown.

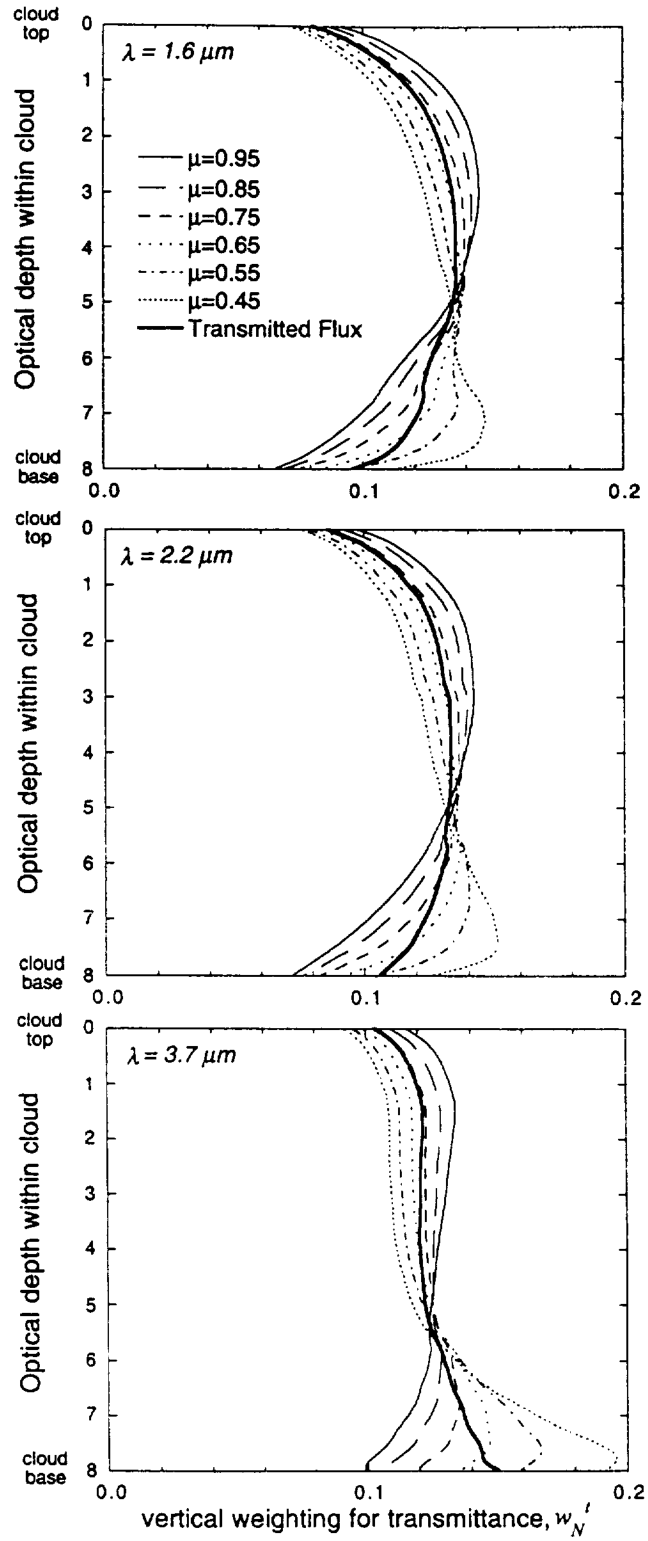

Fig. 5b. Same as Fig. 4a, but for the bidirectional and flux transmittance weighting function w_N^t.

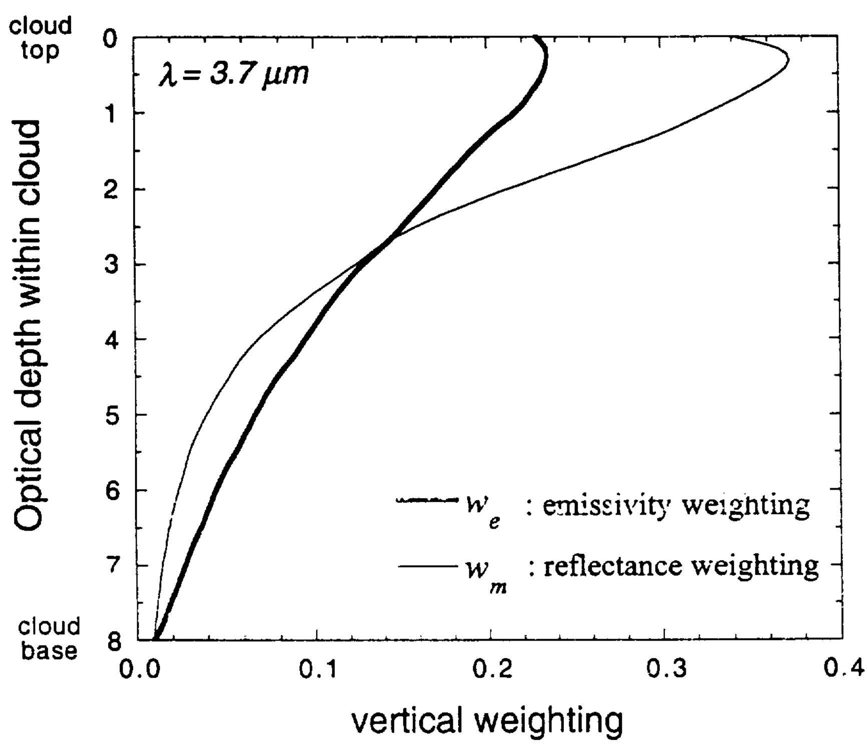

Fig. 6. Example of normalized reflectance and emissivity weightings for a 3.7 μm channel. Calculated for a cloud with a total optical thickness of 8, effective radius varying as from 5 μm at cloud base to 12 μm at cloud top with profile *C* in Table 1, cosine of solar zenith and viewing angles of μ_0=0.65 and μ=0.85, respectively, and an azimuthal average. Though the curves are significantly different, the weighting-derived effective radii (Eq. 3) differ by only a few tenths of a micron for the profile chosen.